Pore network modeling of thin water film and its influence on relative permeability curves in tight formations

Minxia He [a,b], Yingfang Zhou [b, c*] , Keliu Wu [a, *], Yongle Hu [d], Dong Feng [a], Tao Zhang [a], Qing Liu [a], and Xiangfang Li [a]

[a] *State Key Laboratory of Petroleum Resources and Prospecting, China University of Petroleum (Beijing), Beijing 102249, P.R. China*

[b] *School of Engineering, University of Aberdeen, Aberdeen AB24 3UE, United Kingdom*

[c] *State Key Laboratory of Oil and Gas Reservoir Geology and Exploitation, Southwest Petroleum University, Chengdu, Sichuan, China*

[d] *PetroChina Research Institute of Petroleum Exploration and Development, Beijing 100083, China*

[*] *Corresponding author: Yingfang Zhou, E-mail address: yingfang.zhou@abdn.ac.uk*

Keliu Wu, E-mail address: wukeliu19850109@163.com

Abstract

The thin water film stabilized by disjoining pressure is non-negligible in tight formations which results in significant difference in multiphase flow behavior compared with that in conventional formations. In this work, a pore network model is proposed to simulate two phase flow in tight formations to highlight the contribution of thin water film on multiphase flow. The newly developed pore network model includes the influence of thin water film on fluid configuration, capillary entry pressure, fluid conductance and connectivity during multiphase flow in pore space. Our approach is first validated with the existing pore network model and then the influence of thin water film on two-phase flow is investigated extensively. The results show that the connate water saturation increases and its associated oil relative permeability decreases as the average pore radius decreases. It also suggests that in water-wet systems, the influence of thin water film on both oil and water phases becomes significant when the average pore radius is smaller than 100 nm. Existence of thin water film will increase the proportion of film water and corner water, resulting in an increasement in oil phase

relative permeability and a slight decline of water phase relative permeability in tight porous media dominated by angular pores and throats; while in porous media dominated by circular shaped pores and throats, oil and water phase relative permeability are both enhanced due to better connectivity caused by thin water film; at the same time swelling of water film results in lower residue oil saturation and higher end point of water relative permeability. We also found higher water relative permeability when porous media has more irregular pores.

Keywords: Water film, Tight formation, Pore-network modeling, Quasi-static, Multiphase flow

1. Introduction

Tight oil reservoirs have been attracting considerable interests in recent years due to the increasing energy demand and production depletion in conventional reservoirs [1, 2]. Water flooding, which is considered as one of the most feasible secondary recovery approaches, has been adopted to extract hydrocarbon from tight oil reservoirs. However, even implemented with advanced horizontal well and volumetric fracturing strategies, the recovery factor is still not promising as the limitation of relatively poor formation properties of tight formation [3, 4]. Compared with conventional sandstone reservoirs, the pore sizes of tight formations are much smaller and span from micro- to nano-scale [5-8]. Therefore, a rigid understanding of oil-water flow behavior in nano/micro scale pore space plays an important role in evaluating the efficiency of water flooding and favorable production strategy design in tight formation [9].

During primary drainage, a thin water film is often deposited on the water-wet solid surface [10]. Li and He [11] conducted a large amount of experiments to investigate the dependence of water film thickness on pressure gradient and capillary radius in microtubes, and they found that the thickness of water film increases as capillary tube radius or pressure gradient decreases. Based on experimental data, empirical correlations are also established to quantify the thickness of water film [12]. These studies have shown that the thin water film could contribute up to 60% volume of nano-scale pore throat. Furthermore, the stability and thickness of nano-scale thin water film strongly depend on the solid-liquid interaction. In a rock/brine/oil system, the stability and thickness of thin water film are significantly influenced by chemical characteristics of the system including water salinity [13, 14], crude oil composition [14, 15], surface texture [16, 17], temperature [18], pH [19] and so on. Even though the thin water may collapse under some conditions, many researchers have demonstrated that the thin water film could remain stable after primary drainage and the reservoir remain water-wet, especially in tight reservoir [14, 16, 20]. Roman et al. [10] measured the water film thickness and investigated the water film dynamics during drainage process. Results showed that the residing water film leads to snap-off during imbibition process. In addition, using molecular dynamic (MD) simulations, Zhan et al. [21] investigated the effect of water film on oil flow in quartz nanopores. They found that liquid-liquid slip phenomenon could be non-negligible in small nanopores and the thin water film is capable of flowing. These studies have shown that the thin water film has a significant effect on dynamics of the fluid flow in micro/nano tube. Due to the relatively high percentage and reduction of effective flowing space in nanopores, the influence of thin water film on multiphase flow behavior becomes non-negligible [22-25]. Therefore, the impact of thin water film on multiphase flow in tight formation has to be considered properly.

Relative permeability is the key parameter to describe the multiphase flow behaviors, which could be investigated by many methods, such as experiments (steady-state or unsteady-state core flooding tests) [26-29], analytical modeling [22, 30-35], simulations (Lattice-Boltzmann (LB) method, finite element method and pore network modelling [36-39]). For tight formations, the core flooding test method is time consuming and may fail to work due to its low permeability [40]. As analytical methods, capillary bundle model is usually used to determine the relative permeability. Based on capillary bundle model, Zhang et al. [22] investigated the effect of water film on gas-water relative permeability, and they found that water film has a negative impact on both the gas and water phase relative permeability in nano-porous media. Tian et al. [12] improved Purcell's model to estimate oil-water relative permeability in tight oil reservoirs with incorporation of thin water film effect while they didn't consider its flow capability. Wang et al. [32] employed fractal theory to predict gas-water relative permeability in nanoporous media with consideration of interfacial effects. They quantified the contribution of different surface force components and the interfacial effects is proven to promote the fluid flow in the nanoporous media. These analytical models simplified the porous media to capillary tubes with given pore size distribution. However, they fail to capture the topology and complexity of pore space [31, 41, 42]. As simulation methods, Lattice-Boltzmann (LB) method [43, 44] and finite element method could capture the complexity and topology of pore space with time consuming and requires large computation resources [45]. In contrast, pore network modelling representing pore space as nodes interconnected by throats, finds an efficient way to take the complexity of porous media into consideration with acceptable cost of time and resources and has been used extensively to estimate relative permeability curves with the development of recent advanced imaging techniques[46-52].

The pore network modeling could be classified into quasi-static model and dynamic model according to the ratio between viscous force and capillary force during the multiphase flow. When capillary pressure dominates the flow (with capillary number less than 10^{-6}), the quasi-static pore network model is accurate enough to simulate two-phase flow in porous media [45, 53, 54]. To our knowledge, the flow in tight formations is dominated by capillary pressure, therefore the quasi-static pore network model is chosen here. Over the last few decades, the quasi-static pore network model has been proven to be successful in predicting steady-state relative permeability in conventional sandstone [39, 47, 55, 56]. Ruspini et al. [57] and Raeini et al. [38] incorporated more advanced methods into a quasi-static pore network model to calculate cooperative pore-filling pressure. However, these pore network models only took corner water into consideration because of the negligible amount of thin water film attached to the solid surface. As mentioned before, the proportion of thin water films become comparable to non-wetting phase and have flowability in unconventional formations. Thus, it is no longer reasonable to overlook the contribution of these thin water films in tight formations. In order to apply network model to unconventional porous media, some nano-scale phenomena have been introduced into a quasi-static model [58-60]. Nevertheless, no effort has been made about pore network modeling the influence of thin water film on multiphase flow, which is essential in tight formations [12, 61].

Concludingly, the influence of thin water film on multiphase flow is limited in relatively simplified models, such as bundle of capillary tube model, which overlook the pore connectivity and phase trapping. In this work, we aim to include thin water film into quasi-static pore network model to investigate its influence on relative permeability and improve its capacity in predicting oil-water two phase flow in tight formation. First, we introduce the thin water film into the classic quasi-static pore network model; and then we validate the extended pore network model in a Berea sandstone. Subsequently, the effect of pore size and pore shape on relative permeability is studied, from which we can see at what scale the effect of thin water film are unavoidable. Furthermore, the influence of thin water films on relative permeability in tight formation has been investigated thoroughly in terms of connectivity, fluid configuration and flow capability. Our work is then finalized with a short summary and conclusion.

2. Pore network model for tight formations

Quasi-static pore network modeling of multiphase flow requires to adopt an analytical capillary entry pressure as well as fluid conductance together with invasion percolation algorithms to describe displacement in the pre-determined pore network. Previously, pore network modeling has been used extensively to simulate multiphase flow in intermediate and highly permeable rock samples with analytically derived capillary entry pressure and fluid conductance for drainage and followed imbibition processes. In these works, the influence of thin water film on capillary entry pressure and fluid conductance is neglected due to its limited thickness compared with the pore size. It is true that the conductivity of the water film attached on the rock surface is very limited compared with bulk phase flow if the pore size is relatively larger than the water film thickness. While the flow in film couldn’t be neglected when the pore size goes down to nano-scale; this has been supported by amount of previous studies, such as molecular simulation results [21], experimental results [62] and analytical model results [63]. On the other hand, the stability and thickness of thin water film are significantly influenced by water salinity and this could be down by adding salinity into the disjoining pressure model [13, 14]. Because we primarily focus on the scale that water film starts to affect multiphase flow in tight formation, the influence of water salinity is neglected in our study.

In this section, we first describe the qualification of thin water film thickness and the fluid configuration in circular and angular pore throats. And then we include the thin water film thickness into the calculation of capillary entry pressure and fluid conductance during primary drainage and imbibition processes.

2.1. Thin film thickness in nano-scale pore space

The thin water film is often deposited on the water wet solid surface after oil invading into pore space. The residing thin water film could collapse after primary drainage process, and then the oil contact with solid surface directly, which could lead to wettability alteration due to adsorption of polar compounds, the deposition of organic matter and roughness of solid surface and so on [17, 20]. While many researchers have demonstrated that the thin water film could remain stable after primary drainage and the reservoir remain water-wet, especially in tight reservoir [14, 16, 20]; this is because it takes much longer time for the polar molecules in oil phase to adhesive on pore surface through diffusion across the thin water film [64]. The existence of the thin water film (especially in the tight formation) plays a key role in multiphase flow behavior in porous media; this is because first the thin water films increase water film connectivity and thus lead to fluid rearrangements [65], and second the swelling of water films and subsequent snap off displacement during imbibition process reduce oil connectivity [66].

For water-wet circular and angular pore geometry (square or triangular cross section), Fig. 1 presents the possible fluid configurations after primary drainage with water film present. As shown in this figure, the oil phase doesn’t contact with solid surface directly due to the existence of thin water film.

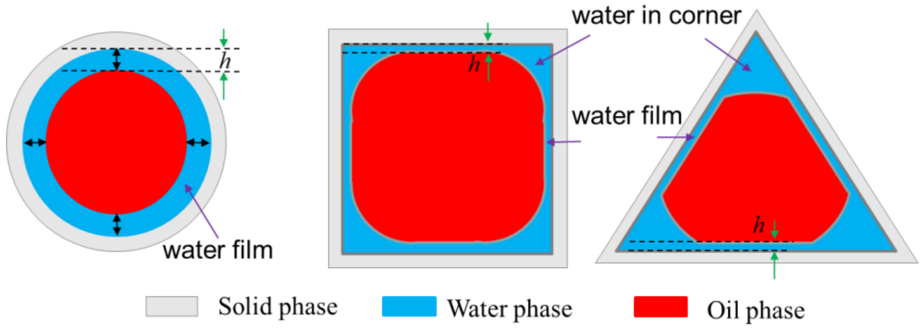

Fig. 1 Schematic of possible fluid configurations, (a) circular pore (b) square pore (c) equilateral triangular pore. Grey: solid, blue: water and red: oil.

The water film shown in Fig. 1 is very thin and is stabilized by the disjoining pressure if the capillary number is very small and the multiphase flow process is dominated by capillary pressure [67]. Due to technical challenge to perform thin film thickness measurement in nano/micro capillary tubes at low capillary number, we have adopted the approach proposed by Derjaguin et al. [68] to estimate the thin water film thickness attached to the water-wet solid wall. This model is based on including the disjoining pressure and capillary pressure with the well-known DLVO theory [13, 68, 69] as below:

$$\prod(h) = \prod_m(h) + \prod_{el}(h) + \prod_{st}(h) \tag{1}$$

Eq. (1) simulates the disjoining pressure as a sum of electrostatic forces between charged surfaces ($\prod_{el}(h)$), the van der Waals force ($\prod_m(h)$), and the structural force ($\prod_{st}(h)$) [70]. In contrast to gas/water/solid system, the Van der Waals force becomes attractive and correspondingly, contributes to negative disjoining pressure and leads to destabilization of the water film [15, 71, 72]. Thus, the other two forces becomes more important in stability of thin water film. The three forces can be formulated as follows:

$$\prod_m(h) = \frac{-A_{ows}(15.96h/l+2)}{12\pi h^3(1+5.32h/l)^2} \tag{2-a}$$

$$\prod_{el}(h) = n_b k_B T\left(\frac{2\zeta_1\zeta_2\cosh(\kappa h)-{\zeta_1}^2-{\zeta_2}^2}{(\sinh(\kappa h))^2}\right)\frac{\varepsilon\varepsilon_0}{8\pi}\frac{(\zeta_1-\zeta_2)}{h^2} \tag{2-b}$$

$$\prod_{st}(h) = A_k e^{-\frac{h}{\lambda}} \tag{2-c}$$

where A_{ows} is the Hamaker constant in an oil-water-solid system, given by Eq.(3), h is the water film thickness; l is the London wavelength; n_b is the ion density in bulk phase; k_B is the Boltzman constant; T is the temperature; ζ_1 and ζ_2 are the zeta potential at solid/water and water/oil interface respectively; A_k is the coefficient for the structural force; λ is the decay length. κ is the Deby-Huckel reciprocal length and can be given by Eq.(4).

$$A_{ows} \approx \left(\sqrt{A_{oo}} - \sqrt{A_{ww}}\right)\left(\sqrt{A_{ss}} - \sqrt{A_{ww}}\right) \tag{3}$$

where A_{oo}, A_{ww}, and A_{ss} are the Hamaker constants of oil/oil, water/water and solid/solid via vacuum, respectively.

$$\kappa = \sqrt{\frac{2e^2z^2n_b}{\varepsilon\varepsilon_0 k_B T}} \tag{4}$$

where e is the electron charge; ε_0 is the dielectric permittivity of vacuum; ε is the relative permittivity of water; z is the ion valence.

As shown in Fig.2, for a circular pore, the pressure difference between oil and water caused by arc meniscus and the disjoining pressure effect is described as [22]:

$$\Delta P = P_o - P_w = \frac{\sigma}{R-h} + \prod(h) \tag{5}$$

Combined with the pressure difference caused by terminal arc meniscus, the relationship between disjoining pressure and thin water film thickness at capillary entry pressure can be formulated as [22]:

$$\frac{\sigma}{R-h} = \prod(h) \tag{6}$$

where P_o and P_w is the oil phase pressure and water phase pressure, respectively; σ is the oil/water interfacial tension; R is the radius of tube; h is the water film thickness. However, once oil is displaced, the terminal meniscus no longer exists. Eq. (5) will be used to describe the relationship between disjoining pressure and thin water film thickness.

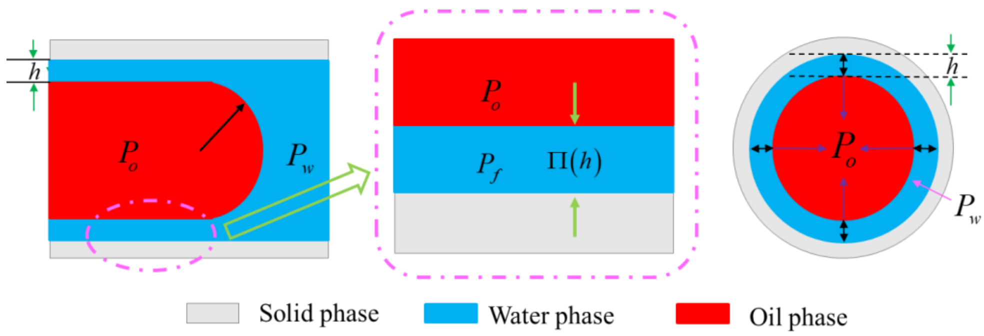

Fig. 2 Schematic diagram of force analysis during drainage process in a circular tube

As shown in Fig. 3, the relationship between pressure difference and disjoining pressure in angular pores can be expressed as [73]:

$$\frac{\sigma}{r_{ow}} = \Pi(h) \tag{7}$$

where r_{ow} is the capillary radius of arc meniscus.

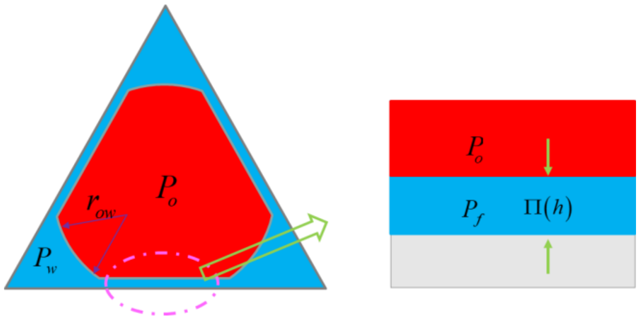

Fig. 3 Schematic diagram of force analysis during drainage process in an angular pore

From Eqs. (1-7), it can be seen that film thickness is a function of pore radius and capillary pressure which is consistent with that obtained by experiments [61]. In the calculation of water film thickness, the values of these parameters are shown in Table 1 with reference to previous experimental studies.

Table 1 Summary of parameters used in the calculation

Parameter	Symbol	Unit	Value
Hamaker constant of oil/oil	A_{oo}	J	5×10^{-20} [70]
Hamaker constant of water/water	A_{ww}	J	3.7×10^{-20} [70]
Hamaker constant of solid/solid	A_{ss}	J	6.5×10^{-20} [70]
London wavelength	l	nm	100 [70]
Ion valence	z	Dimensionless	1
Electron charge	e	C	1.6×10^{-19}
Boltzmann constant	k_B	J/K	1.38×10^{-23}
Temperature	T	K	298
Dielectric permittivity of vacuum	ε_0	F/m	8.854×10^{-12} [13]
Relative permittivity of water	ε	Dimensionless	78.4 [13]
zeta potential at solid/water interface	ζ_1	mV	-80 [19]
zeta potential at water/oil interface	ζ_2	mV	-70 [19]
Coefficient for the structural force	A_k	Pa	3.3×10^{10} [19]
Decay length	λ	nm	0.6 [19]
Interfacial tension	σ	mN/m	25 [16]

2.2. Capillary entry pressure calculation

Pore network modeling requires the capillary entry pressure as a priority to be implemented for fluid invasion in the pore network [74]. Here in this work, we considered the thin water film attached on the water-wet rock surface, and we first simulate the primary oil displaces water in water-filled pore networks, which is referred to as primary drainage process. The primary drainage process is then followed by waterflooding process until the capillary pressure reaches its minimum or the water saturation reaches the target water saturation. Saturation can be calculated at any point

$$S_{w,t} = \frac{\sum_{i=1}^{N} V_i S_{w,i}}{V_t} \tag{8}$$

where $S_{w,t}$ is the water saturation of the network, $S_{w,i}$ and V_i are the water saturation and volume of a pore throat, N is the total number of pores and throats, and V_t is the total volume of the network.

Applying mass conservation at every pore, the flow rate of each phase is then estimated by solving the pressure distribution throughout the network

$$\sum_j q_{ij} = \sum_j g_{ij}\left(P_i - P_j\right) = 0 \tag{9}$$

where j is the number of throats connected to pore i, q_{ij} and g_{ij} are flow rate and flow conductance respectively between pore i and pore j, P_i and P_j are pressure of pore i and pore j.

The conductance between two pore elements g_{ij} can be calculated by harmonic mean method as follows

$$\frac{L_{ij}}{g_{ij}} = \frac{L_i}{g_i} + \frac{L_t}{g_t} + \frac{L_j}{g_j} \tag{10}$$

where t indicates the connecting throat, L_i and L_j are the lengths from the pore-throat interface to the pore center.

2.2.1. Drainage process

The capillary entry pressure of oil invades a water saturated circular capillary tube could be estimated by the Young-Laplace equation [73]:

$$P_{entry} = \frac{2\sigma \cos\theta_{ow}}{R-h} \tag{11}$$

where σ is oil-water interfacial tension, R is radius of element, θ_{ow} is the contact angle and h is the thin water film thickness.

The MS-P method [75-82] was initially proposed to calculate capillary entry pressure in straight tubes based on free energy balance. For polygon geometry, the capillary entry pressure for oil invasion could be estimated by Eq. (12) and the details of the calculation are shown in the Appendix. It has to be noticed that the new analytical model has a similar expression with the previous models which possess simple and concise forms. Specifically, the effect of thin water film is incorporated to calculate the capillary entry pressure.

$$P_c = \frac{\sigma\left(\sqrt{1+4GD}+1\right)}{r_a} \tag{12}$$

where $G=A/L^2$ is the shape factor, $r_a = R-h$ is the oil inscribe maximum radius and D is defined as：

$$D = \sum_{k=1}^{n}\left\{\frac{\pi}{2} - \theta_{ow} - \alpha_k\right\} + cos\,\theta_{ow}\sum_{k=1}^{n}\frac{cos(\theta_{ow}+\alpha_k)}{sin(\alpha_k)} \tag{13}$$

where n is corner number of the pore; α_k is the corner half angle.

2.2.2. Imbibition process

In the water imbibition process, piston-like displacement is a major displacing mechanism. As capillary pressure decreases gradually, due to contact angle hysteresis the oil-water interface in corner remains pinned at the initial position of imbibition with hinging contact angle $\theta_{h,k}$. When advancing contact angle θ_a is reached, the oil-water interface starts to move. When the capillary pressure is positive, the threshold capillary pressure for piston-like displacement can again be calculated based on the principle of interfacial energy balance. The following formula can be solved iteratively to obtain the capillary entry radius.

$$r_{ow} = \frac{A_o}{L_{ow}+L_{os}\cos\theta_a} \tag{14}$$

$$A_o = \frac{r_a^2}{4G} - \sum_{k=1}^{n} r_{ow}^2\left\{\theta_{h,k} + \alpha_k - \frac{\pi}{2} + cos\left(\theta_{h,k}\right)\frac{cos(\theta_{h,k}+\alpha_k)}{cos(\alpha_k)}\right\} \tag{15}$$

$$L_{os} = 0 \tag{16}$$

$$L_{ow} = 2r_{ow}\sum_{k=1}^{n}\operatorname{asin}\left(\frac{b_k\sin\alpha_k}{r_{ow}}\right) + \frac{r_a}{2G} - 2\sum_{k=1}^{n} b_k \tag{17}$$

$$b_k = r_{ow}\frac{cos(\theta_a+\alpha_k)}{sin\,\alpha_k} \tag{18}$$

where A_o is the area occupied by oil, L_{ow} is the length of oil-water interface, L_{os} is the length of the solid-water interface, $\theta_{h,k}$ is the hinging contact in a corner, b_k is the length from three phase contact point to corner apex as shown in Fig. A 1, and θ_a is the advancing contact angle.

Besides piston like displacement, cooperative pore-filling plays an important role during the imbibition process. The capillary entry pressure for filling a pore dependents on the number of adjacent oil filled throats and contact angle [54, 83, 84]. Recently

Ruspini et al. [57] presented a new algorism to calculate pore filling capillary pressure which overcomes the uncertainty of stochastic models. Since we mainly focus on the effect of thin water film on relative permeability, for simplicity we include the thin water film in the well-known pore filling model proposed by Blunt et al. [85] to estimate the entry pressure for pore filling events:

$$P_c = \frac{2\sigma \cos\theta_a}{(R-h)} - \sigma \sum_{i=1}^{m} B_i x_i \tag{19}$$

$$B_2 - B_m = \frac{0.03}{\sqrt{K}} \tag{20}$$

where m is the number of adjacent non-wetting phase filled throats, x_i are random weight coefficient numbers ranging from zero to one, B_i are arbitrary numbers and K is the permeability.

2.3. Conductance calculation

In order to calculate single and multiphase permeability during drainage and imbibition, the phase conductance should be cooperated with given a fluid configuration determined using capillary entry percolation algorithm. The conductance for single-phase flow in a capillary tube with no-slip boundary has been described as a linear function or second-order polynomial equation of shape factor [56, 86]. In this work, the linear correlation is used to calculate the single-phase conductance as below:

$$g_p = k\frac{A^2 G}{\mu_p} \tag{21}$$

where k=0.5 for circular, k=3/5 for triangles and k=0.5623 for squares [45], A is area of cross-section and μ_p is the fluid viscosity.

2.3.1. Conductance of two-phase flow in circular pores

The water-oil distribution in micro/nano pores is assumed to be that water phase flows in the outer annulus and oil phase in the core as shown in Fig. 1a. The volume flux of each phase can be given by following expression respectively [87]:

For simplicity, we can define oil radius in tube as r_a=R-h.

$$q_o = \frac{\Delta p}{L}\frac{\pi {r_a}^4}{8\mu_o} + \frac{\Delta p}{L}\frac{\pi(R^2 - {r_a}^2){r_a}^2}{4\mu_w} \tag{22-a}$$

$$q_w = \frac{\pi \Delta p}{8\mu_w L}(R^2 - {r_a}^2)^2 \tag{22-b}$$

where r_a=R-h is the radius of oil phase.

From Eq. (22) we can get conductance of each phase as follows:

$$g_{co} = \frac{\pi {r_a}^4}{8\mu_o} + \frac{\pi(R^2 - {r_a}^2){r_a}^2}{4\mu_w} \tag{23-a}$$

$$g_{cw} = \frac{\pi}{8\mu_w}(R^2 - {r_a}^2)^2 \tag{23-b}$$

where μ_w denotes for water viscosity and μ_o denotes for oil viscosity.

The water saturation is presented as follows:

$$S_{w,i} = 1 - \frac{{r_a}^2}{R^2} \tag{24}$$

2.3.2. Conductance of two-phase flow in angular pores

During drainage process oil phase occupies the central area of the pore throat, while water phase exists in the corner and as thin film along the water-wet surface (see Fig. 3). During imbibition process oil layers doesn't exist under assumption of water-wet network according to oil layer formation criteria [86, 88]. So taking scenario shown in Fig. 3 as an example, we calculate area and conductance for bulk oil, corner water and water films respectively.

The correlation proposed by Oren [56] is adopted in our work to describe the flow of corner water. With consideration of water film, the area of the water phase in the corner needs to be revised by adding the trapezoid part as shown in Fig. A 1 and formula is given by:

$$g_{pc} = C\frac{A_c^2 G_c}{\mu_w}, C = 0.364 + 0.28\frac{G_c^*}{G_c} \tag{25}$$

$$A_c = r_a^2\left\{\theta_{ow} + \alpha_k - \frac{\pi}{2} + cos(\theta_{ow})\frac{cos(\theta_{ow}+\alpha_k)}{sin(\alpha_k)}\right\} + h(2b_i + h\cot\alpha_k) \tag{26}$$

where G_c is the shape factor for the pore throat which contains the film, G_c^* is the shape factor with zero curvature on the oil-water interface, A_c is corner water area and μ_w is the water viscosity.

Conductance of thin water films could be estimated by the slit flow equation [89]:

$$g_{pf} = \frac{A_f h^2}{12\mu_w} \tag{27}$$

$$A_f = L_{of} h \tag{28}$$

where A_f is water film area and L_{of} is length of water film.

The bulk oil phase conductance is estimated by multiplying the single-phase conductance by the percentage the bulk phase occupies [88].

$$g_{po} = \frac{A_o}{A} g_p \tag{29}$$

$$A_o = A - A_c - A_f \tag{30}$$

The water saturation is given by

$$S_{w,i} = 1 - \frac{A_o}{A} \tag{31}$$

3. Results and discussion

We first validate our extended pore network model using the measured relative permeability curves in Berea sandstone core samples. To better analyze the effect of thin water film on relative permeability, the influence of thin water film on capillary entry pressure, fluid configuration and fluid conductance in a single pore are is investigated. And then we qualify the dependency of relative permeability on average pore size and pore shape and illustrate the effect of thin water film on relative permeability.

3.1. Model validation

Here we use the network generated from reconstructed Berea sandstone [90] to validate our pore network model, the pore network is generated with the well know maximum ball algorithm proposed by Dong et al [91]. The pore throat size distribution is shown in Fig. 4. Relative permeability curves during drainage and imbibition process are predicted using our extended model and Valvatne's model [88]. During primary drainage process the network is assumed to be strongly water wet with an intrinsic contact angle of zero degree. During imbibition process, due to wettability alteration and surface roughness [92], the advancing contact angles have a significant influence on relative permeability prediction [93] and we assign it a uniform distribution between 50 and 60 degrees as in Valvatne's prediction [88]. The simulated and experimental relative permeability curves are shown in Fig. 5. It can be seen that curves simulated by our proposed model achieve good agreement with experimental data and Valvatne's prediction, especially for the oil phase relative permeability. Therefore, the validation results prove the reliability of the proposed pore network model. It can also be observed that in this case effect of thin water film on relative permeability is negligible. This is because the thin water films have thicknesses ranging from 10nm to 40nm (see Fig. 6), and thus they have very limited influence on multiphase flow behavior as the thin water film is much smaller than the pore size as given in Fig. 4.

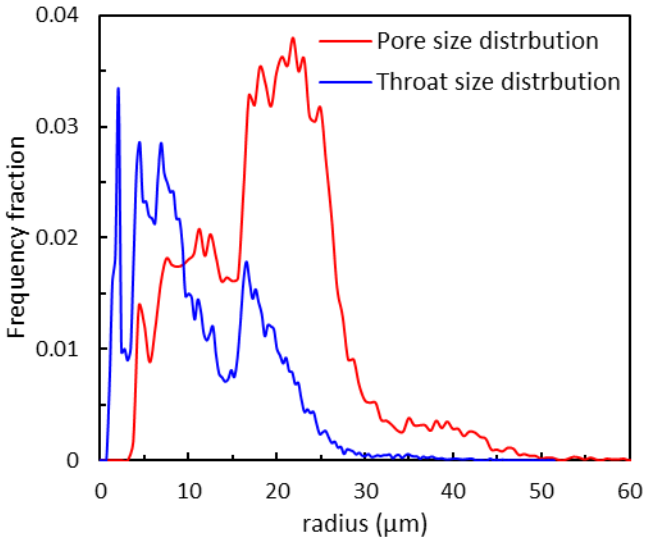

Fig. 4 Pore throat size distribution curves of the Berea sandstone [90]

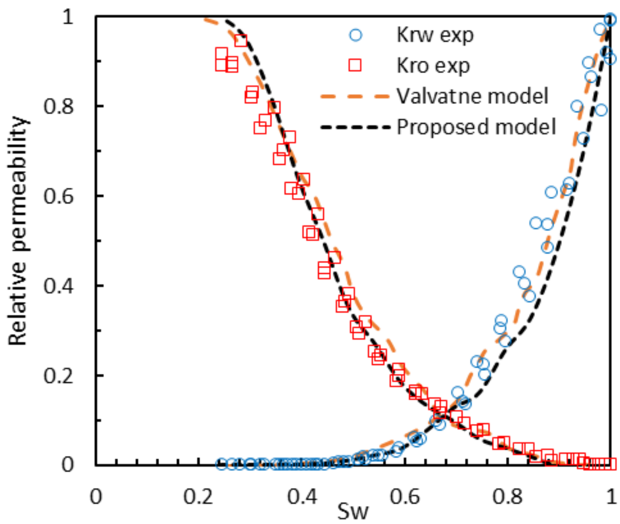

(a) in drainage process

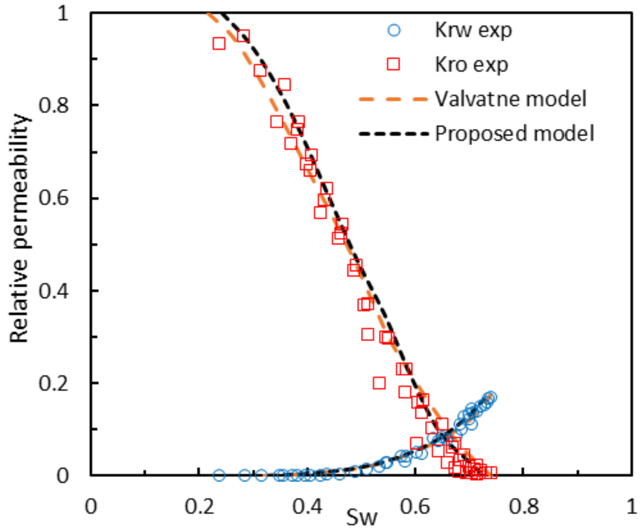

(b) in imbibition process

Fig. 5 Relative permeability curves: experiment data by Oak [94] and predicted results from the proposed network model

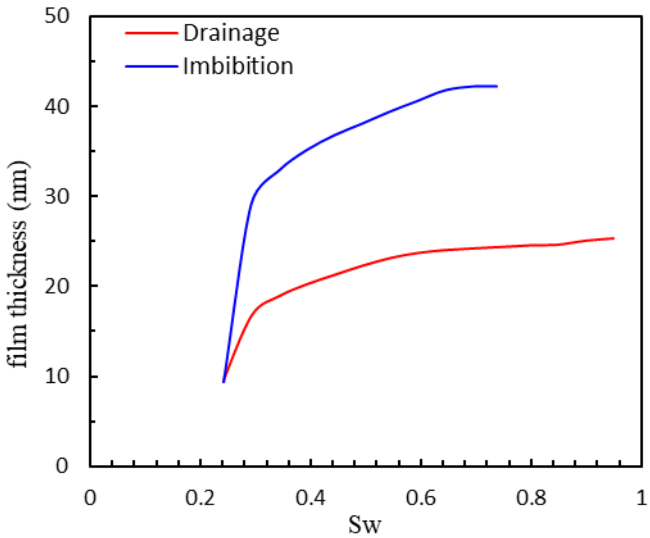

Fig. 6 Thickness of thin water film during drainage process and imbibition process

3.2. The influence of thin water film on flow behavior in capillary tube

3.2.1. The influence of thin water film on fluid distribution

In order to characterize the effect of thin water film on fluid distribution, we investigate the thickness of thin water film at capillary entry pressure. The effect of pore throat radius on thin water film thickness and water saturation at capillary entry pressure during drainage process is shown in Fig. 7. As pore radius increases, the thickness of water film at capillary entry pressure attached to solid wall becomes thicker, and as expected the water saturation becomes smaller. When the radius reaches 100 nm, the influence of thin water film on water saturation can be negligible. At the same inscribed radii, pores with circular-cross section have thicker water films than that with angular cross-section, and the difference increases when pore radius increases. However, the relationship between water film thickness and pore size at a given capillary pressure value varies in circular pores and polygonal pores. For circular pores, the water film thickness will decrease with increasement of pore radius. However, for polygonal pores, the water film thicknesses are identical due to the same capillary pressure.

Besides, the contributions of thin water film and corner water to the total water saturation for angular pores are shown in Fig. 8. In this figure, the water saturation curves without thin water films are also presented to compare the influence of thin water film on water saturation. It can be seen that the thin water film is critical for evaluating water saturation in small-sized pores (e.g. r <100nm). The traditional model (without considering the thin water film) underestimates the total water saturation in small pores due to the existence of thin water film. While on contrast, it slightly overestimates the total water saturation in large pores. That's because the water saturation contributed by thin water film gradually approaches zero in large pores. However, the thin water film slightly increases the threshold capillary pressure and thus slightly decreases the saturation of corner water.

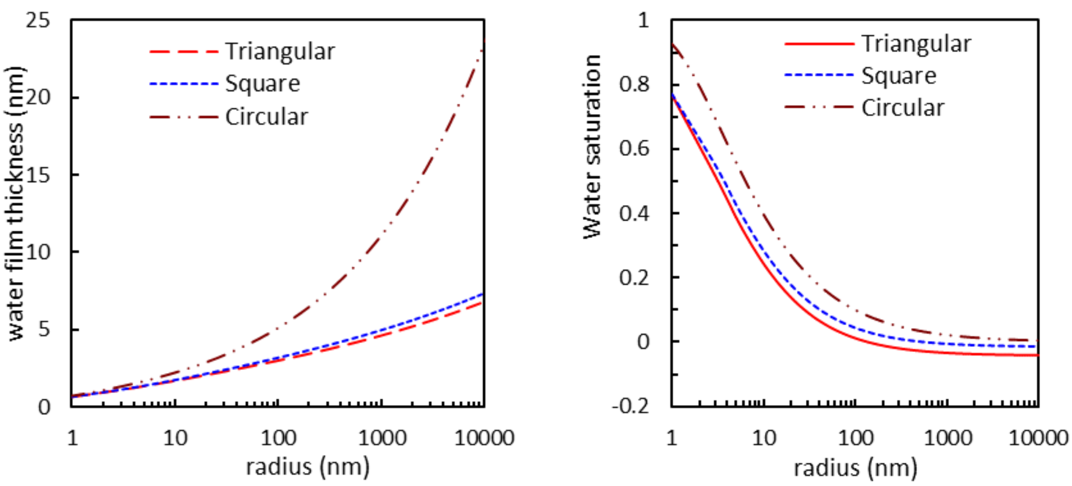

(a) thickness of thin water film (b) water saturation at capillary entry pressure

Fig. 7 Thin water film thickness residing on the wall at capillary entry pressure and its influence on water saturation

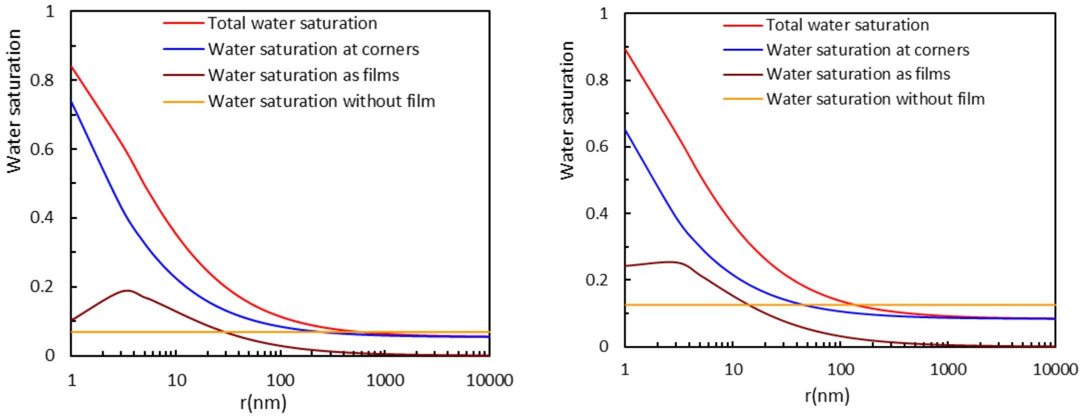

(a) square pore (b) triangular pore

Fig. 8 Contribution of water at corners and water film om total water saturation for (a) square pores (b) triangular pores

Previous studies have shown that the thickness of thin water film is not a constant value during displacement, for example it strongly depends on applied pressure gradient [11]. In quasi-static pore network model, the fluid configuration is estimated for each pre-set capillary during the displacement processes. Thus, the relationship between thin water film thickness and capillary pressure in various shaped pores is discussed for three cases with pore radii equal to 10, 50 and 100 nm.

Fig. 9 presents that the effect of capillary pressure on thin water film during drainage process can be basically divided into three stages. When less than threshold pressure P_{entry} (the stage I), the capillary pressure has no effect on thin water film thickness. It is because that there exists only wetting phase in the pores. Non-wetting phase invades into pores only if capillary pressure reaches capillary entry pressure. When the capillary pressure exceeds entry pressure (the stage II), the water film thickness drops straightly due to invasion of non-wetting phase and after that they decrease dramatically with an increase in capillary pressure. Eventually, when the thin water film becomes thin enough (the stage III), the capillary pressure has little effect on water film thickness. The reason is that at this time the film is mainly controlled by attraction force between water molecular and solid surface. Correspondingly the relationship between capillary pressure and water saturation is shown in Fig. 10. When the capillary pressure reaches entry pressure, water saturation decreases suddenly, and with further increasement of capillary pressure it has a dramatic decrease. Eventually, near the irreducible water saturation, the capillary pressure curves become nearly vertical.

In imbibition process, the relationship between thin water film thickness and capillary pressure is similar to that of drainage process. Corresponding to the non-wetting phase invasion, the wetting phase collapse is essential in imbibition process. The thin water film becomes unstable at the critical thickness and results in spontaneous coalescence. The collapse of water film occurs when the pressure partial differential $\partial p/\partial h<0$ [95] [96]. Based on Eq. (5) and Eq. (7) the critical thickness of thin water film can be expressed by Eq. (32) for circular pores and Eq. (33) for angular pores. Its relationship with pore throat radius is shown in Fig. 11. Compared with Fig. 7, it can be observed that the critical thickness of thin water film during imbibition process is larger than that at capillary entry pressure during drainage process. This is because the non-wetting phase needs larger capillary pressure to invade into pores which means thinner thin water film thickness. It also has to be noted that that critical thickness inside circular pores is larger than that inside angular pores which follows the same trend with Li et al.'s study [73] in the gas-water system.

$$\frac{\sigma}{(r-h)^2} + \Pi'(h) = 0 \tag{32}$$

$$\frac{\sigma}{R-h} = \Pi(h) \tag{33}$$

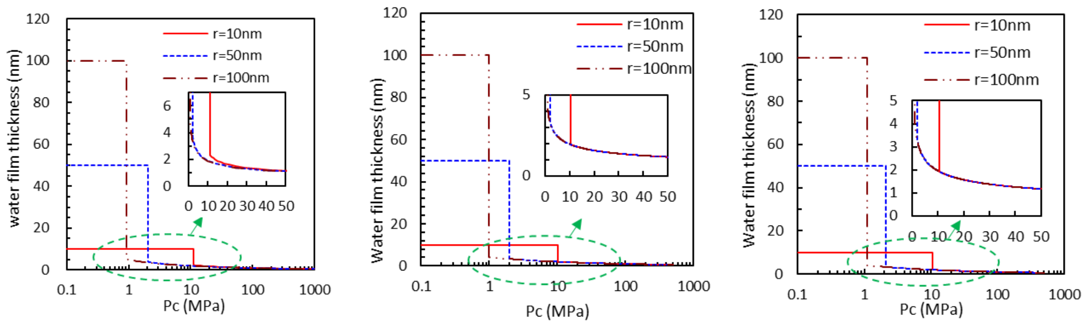

(a) circular pores (b) square pores (c) triangular pores

Fig. 9 Effect of capillary pressure on thin water film thickness during drainage process in various shaped pores

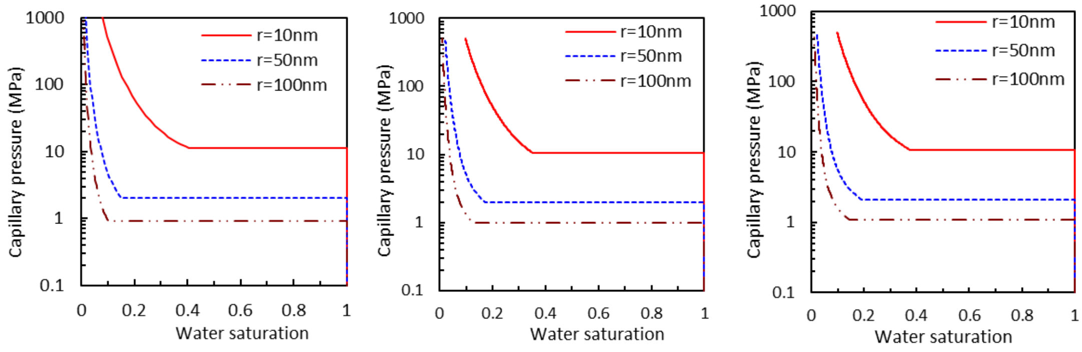

(a) circular pores (b) square pores (c) triangular pores

Fig. 10 Capillary pressure curves in various shaped pores

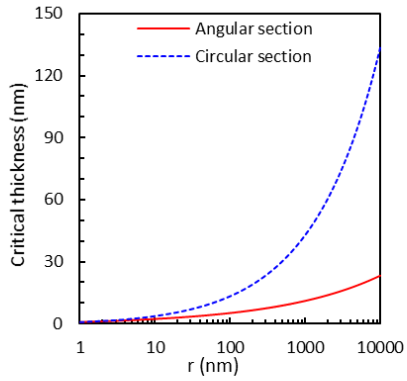

Fig. 11 Critical thickness of thin water film during imbition process

3.2.2. The influence of thin water film on capillary entry pressure

The effect of thin water film on capillary entry pressure is analyzed here, as shown in Fig. 12. As shown in this figure, the influence of thin water film on capillary entry pressure is unavoidable if the pore size is smaller than 20 nm. Without considering the thin water film, the traditional models underestimate the capillary entry pressure dramatically. This is because due to the existence of thin water film, the effective flow radius is less than the actual radius of the pore.

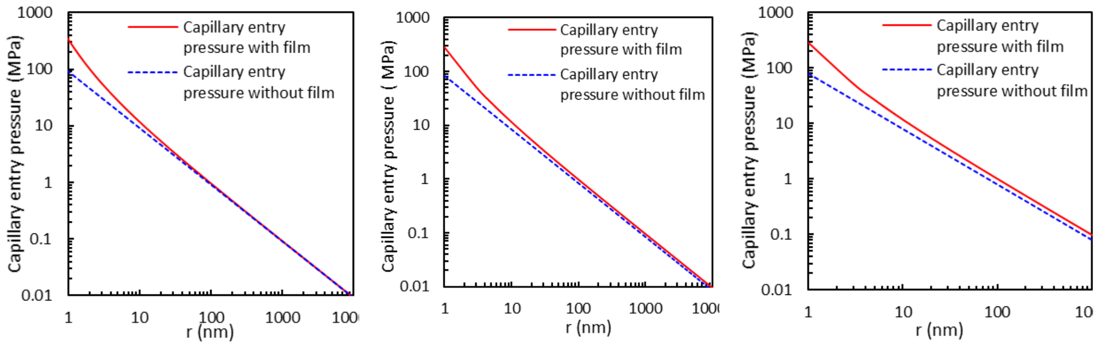

(a) circular pores (b) square pores (c) triangular pores

Fig. 12 Effect of water film on capillary entry pressure inside various shaped pores

3.2.3. The influence of thin water film on phase conductance in pore throat

In order to evaluate the water-oil flow capacity in a single pore with different cross-sections, relative conductance of each phase is defined as:

$$C_t = C_w + C_o \quad (34)$$

$$C_{rw} = \frac{C_w}{C_t} \quad (35)$$

$$C_{ro} = \frac{C_o}{C_t} \quad (36)$$

The effect of thin water film on relative conductance of each phase and its sensitivity to pore radii is plotted in Fig. 13. Here the film thickness is assumed to be at entry condition. We can find that the water relative conductance is approximately zero without consideration of water film existence, while the oil conductance approaches to the conductance of single-phase flow through the pore throat. In larger pores this assumption might be appropriate (e.g. for angular pore larger than 20 nm, and for circular pores larger than 100 nm). However, the thin water film plays an important role in smaller pores, especially if the pore size is smaller than 10nm for angular pores and 20nm for circular pores. The relative water conductance increases with a decrease in pore radius while for oil phase decreases.

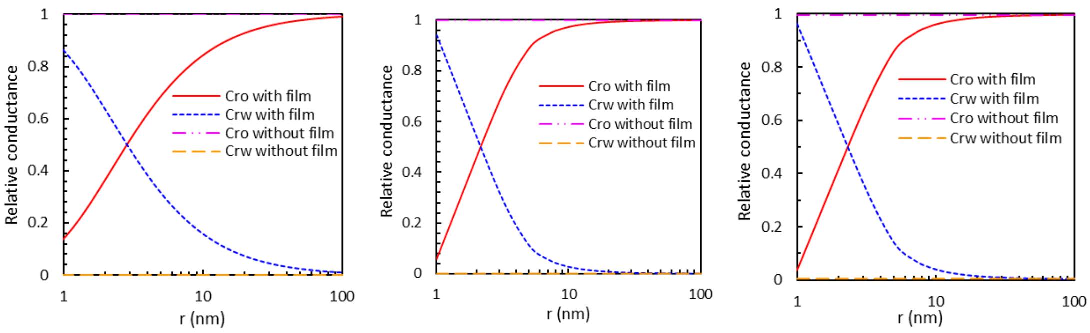

(a) circular pores (b) square pores (c) triangular pores

Fig. 13 Effect of water film on relative conductance inside single pore with various shaped cross-section

3.3. The influence of pore size on relative permeability

As discussed in previous sections, the thin water film influences the capillary entry pressure as well as phase conductance significantly when the pore throat reaches to tens of nanometers, while it is still not clear to us how the thin film affects the multiphase flow process in a complicated pore network. Here, the pore-network extracted for the

Berea sandstone and its downscaled pore-networks are used to understand the influence of thin water film on multiphase flow process at different average pore sizes. The original extracted pore network using the maximum ball algorithm [90] is scaled down by multiplying its physical size by $1/10^{th}$, $1/100^{th}$, $1/200^{th}$, $1/400^{th}$ and $1/700^{th}$ respectively. As a result, all networks have the same porosity which is 0.183 and connectivity, and other basic properties for these rescaled networks are listed in Table 2.

Table 2 Fundament properties for the scaled-down pore networks

Network	Permeability (mD)	Mean pore radii (μm)	Mean throat radii (μm)
Original pore network	2551.6	19.2	11.0
Scaled-down by $1/10^{th}$	2.836	1.92	1.10
Scaled-down by $1/100^{th}$	0.709	0.192	0.110
Scaled-down by $1/200^{th}$	0.315	0.096	0.055
Scaled-down by $1/400^{th}$	0.177	0.048	0.028
Scaled-down by $1/700^{th}$	0.005	0.027	0.016

The relative permeability curves predicted from our extended pore network model during drainage and imbibition process are plotted in Fig. 14. It can be seen that pore size has little effect on relative permeability during drainage process, which is shown in Fig. 14a, b. However as shown in this Fig. 14c, in imbibition process, when the average pore radius increase, the two-phase flow region shifts to the left. High permeable rock sample tends to yield more shrunk relative permeability curve, as the proportion of water film becomes lower. However, pore size has a very limited influence on normalized relative permeability curves (see Fig. 14d). In addition, we also employ Valvatne's model [88] to predict relative permeability for these scaled down networks. However, the relative permeability curves of scaled-down networks predicted by Valvatne's model are the same as that of no-scaled down Berea sandstone which implies it fails to capture the dependence of relative permeability curve on pore size. That's because if there's no water film, similar fluid configuration and relative conductance will be obtained for a given saturation if capillary dominated flow is assumed even pore size varied, but it will be at different capillary pressure. In order to compare the performance of these two models in tight formation, we take the downscaled pore-network by 1/700th as an example and compare the results predicted by these two models. As shown in Fig. 14e, the connate water saturation and end-point relative permeability to water are higher in our proposed model than Valvatne's model due to existence of water film. Our extended model successfully captures the characteristics of relative permeability in tight formations.

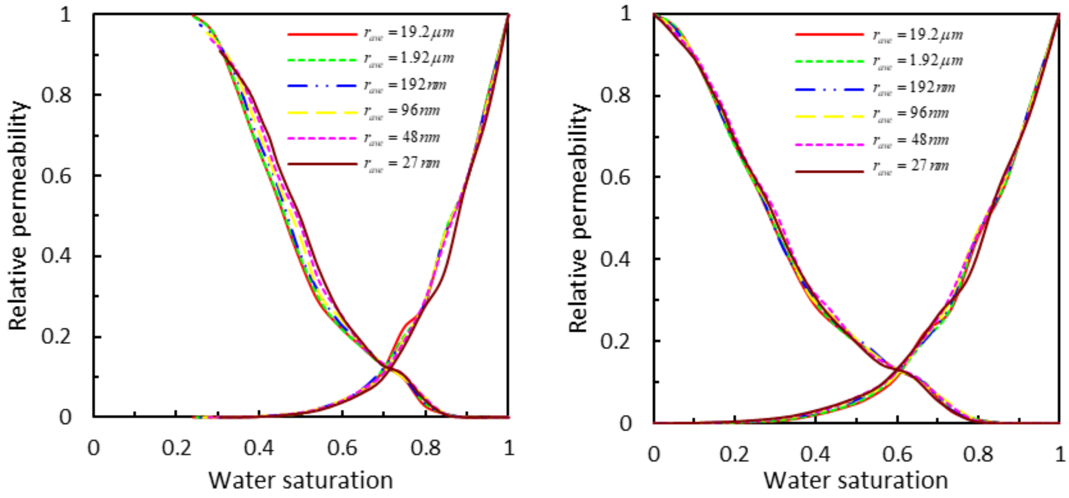

(a) curves of drainage (b) normalized curves of drainage

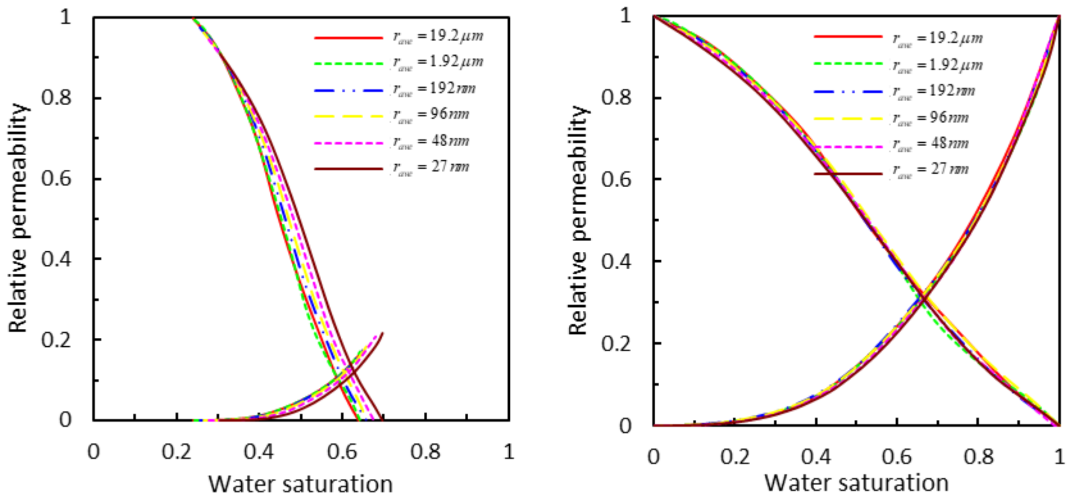

(c) curves of imbibition (d) normalized curves of imbibition

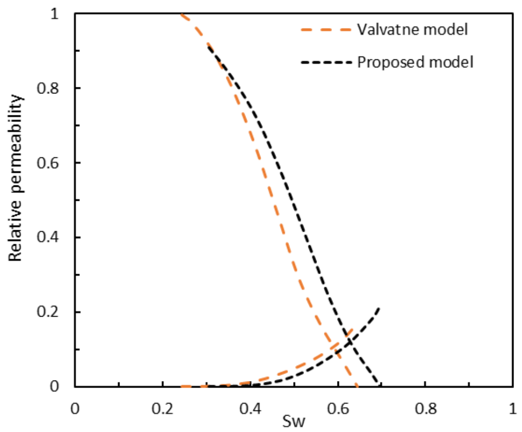

(e) relative permeability curves of imbibition for Berea downscaled pore-network by 1/700th

Fig. 14 The influences of pore size on relative permeability curves

The result also shows that the pore size primarily changes the endpoints of relative permeability as shown in Fig. 15. When the average pore size is smaller than 100 nm, the connate water saturation increases dramatically while oil relative permeability at connate water saturation decreases significantly. This is mainly caused by the fluid configuration distribution in pores. In order to compare fluid configuration in different average pore size cases, we normalize pore throat radius according to the maximum and minimum radius. Fig. 17a shows the water saturation distribution at connate water saturation in different average pore sizes. As average pore size decreases, the water saturation increases which is more conspicuous in small pores. This finding is consistent with previous research by Torskaya et al. [97]. Using lattice-Boltzmann method, they studied the relationship between irreducible water saturation and permeability. They found that permeability decreases with increasing irreducible water saturation.

Meanwhile higher connate water saturation means lower initial oil saturation which leads to lower residual oil saturation as shown in Fig. 16 and this is reasonable under the same porous medium structure. From Fig. 17c, d we can see that in the imbibition process water mainly displaces oil in the sequence of from small pores to large pores due to the dominance of capillary pressure. As average pore size decreases, more pores are displaced by water due to swelling of thin water film. From Fig. 17b we can also find in the oil filled pores the water saturation increases as the average pore radius decreases. As a consequence, water saturation at the end of imbibition process increases with decrease of average pore radius and leads to an increasement of water relative permeability especially when the average pore size is smaller than 100 nm (as Fig. 15 show).

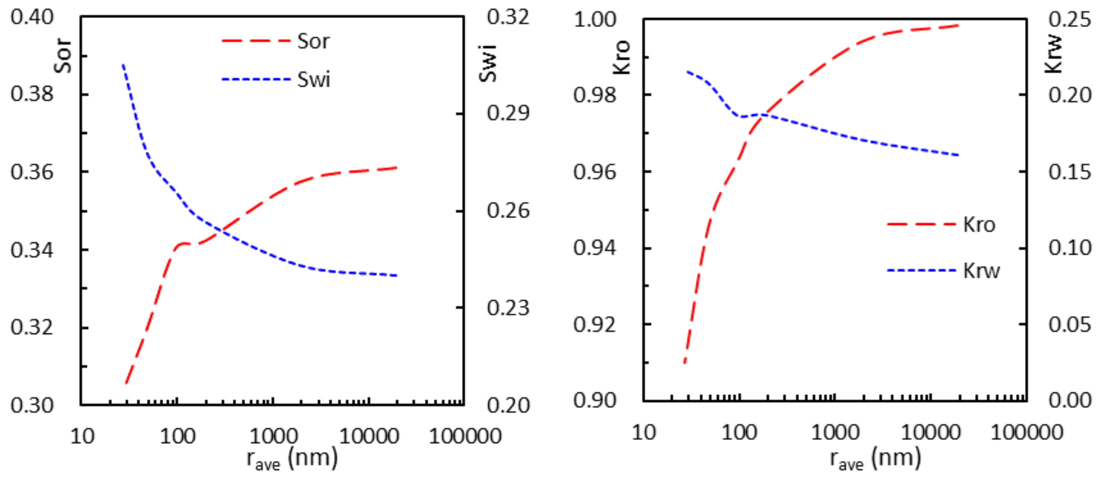

(a) connate water saturation and residue oil saturation

(b) endpoint phase permeability

Fig. 15 Endpoint of relative permeability curves for different permeable core samples during imbibition process

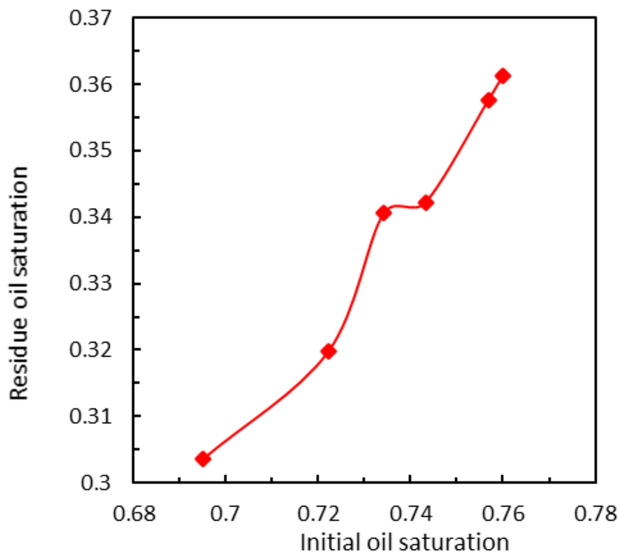

Fig. 16 Relationship between residual oil saturation and initial oil saturation

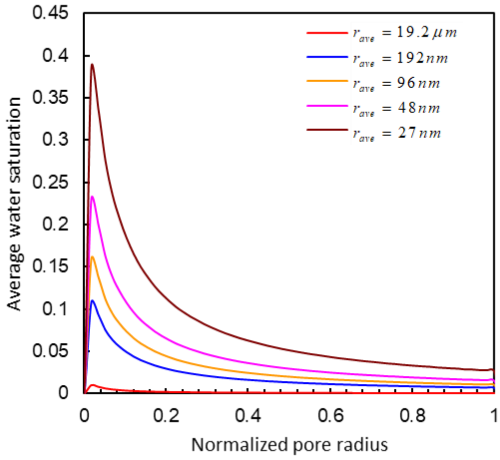

(a) water saturation distribution at connate water saturation

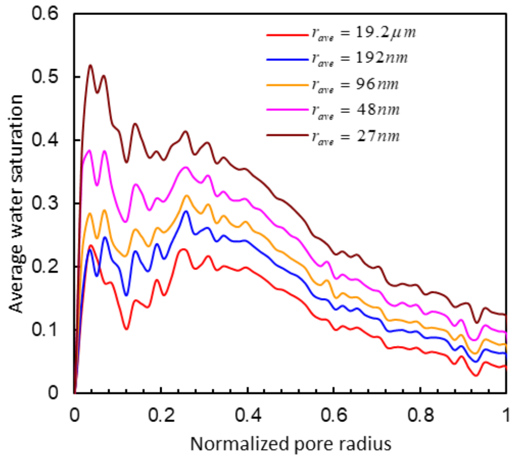

(b) water saturation distribution at residue oil saturation

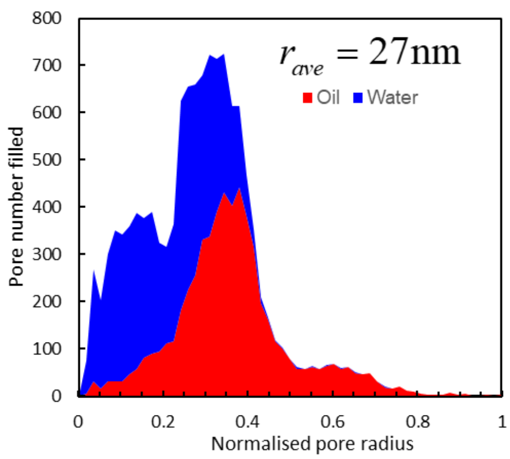

(c) pore number occupied by oil and water in the scaled-down by 1/700th case at residue oil saturation

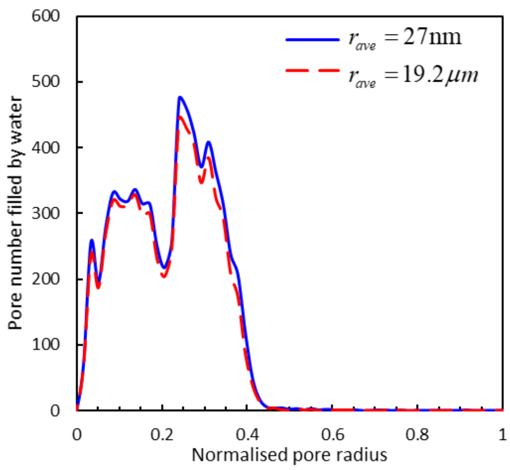

(d) pore number displaced by water under different average pore radius at residue oil saturation

Fig. 17 Effect of average pore size on fluid and water saturation distribution

3.4. The influence of pore shape on relative permeability

As discussed in previous Section 3.2, pore shape is one of the most important factors to determine the relative permeability. Here we use shape factor to characterize pore throat shape which is defined as the cross area divided by the perimeter squared. A low shape factor indicates a highly irregular pore. Normal distribution function is adopted to describe the distribution of pore throat shape factor. Assuming a constant standard deviation is 0.005, the mean shape factors are set to 0.03, 0.04, 0.05 and 0.06 respectively (as shown in Fig. 18). The networks are generated on the basis of Berea downscaled pore-network by 1/700th. In order to compare the flow characteristic on the same flow area, the radii of the downscaled pore-network are calculated according to the shape factor. Thus, these networks have the same porosity as the Berea sandstone and have different absolute permeabilities as shown in Table 3.

Table 3 Fundament properties for the networks with various shape factor distribution

Properties	Mean shape factor (Dimensionless)	Porosity (Dimensionless)	Permeability (mD)
Case1	0.03	0.183	0.0052
Case2	0.04	0.183	0.0069
Case3	0.05	0.183	0.0076
Case4	0.06	0.183	0.0095

The relative permeability curves predicted by our extended pore network model are shown in Fig. 19. The result shows that the water relative permeability increases with the increase of pore irregularity. However, the oil relative permeability is enhanced slightly at a given saturation. This characteristic is mainly dominated by the existence of corner water and snap off event. As the shape factor decreases, the water saturation in a pore throat increases when snap off event happens [73] which results in a low residue oil saturation. On the other hand, snap-off is more likely to occur for more angular throats [98]. At a given water saturation, the proportion of bulk water increases with an increase of the shape factor. However, its connectivity is limited by existence of bulk oil phase. On the contrary, corner water is connected throughout the water-wet network and the increase of corner water proportion will enhance water phase permeability. Therefore, water relative permeability is enhanced with the increase of pore irregularity in networks.

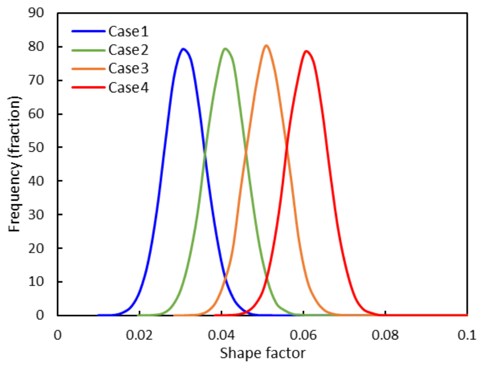

Fig. 18 PSD with various mean shape factor with a constant peak frequency

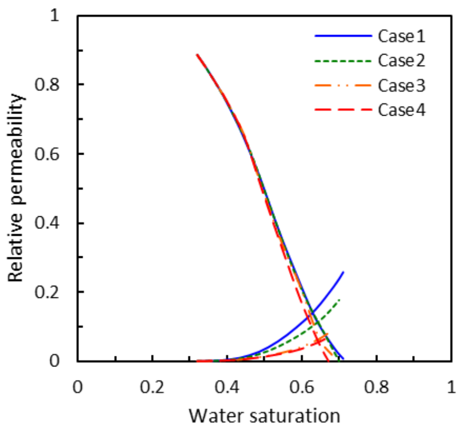

Fig. 19 The effect of shape factor on relative permeability

3.5. The influence of thin water film on relative permeability

It has been noted that the thin water film plays an important role in relative permeability curves of tight formations, while it is not well known how the thin water film affects relative permeability during imbibition process in water-wet rock sample. In this section, we investigate the influence of thin water film in the tight formation with pore size spans over tens of nano meters. The pore network is generated from reconstructed Berea sandstone [90] and then scaled-down by multiplying its physical size by 1/700th, and the average pore and throat radii are 27.4nm and 15.7nm, respectively. The fundamental properties of the pore network are presented in Table 2. The detailed pore throat geometry is presented in Table 4. As shown in this table, the majority of the pores and throats are triangular, and very limited pore and throat with circular.

Table 4 The proportion of each shape in scaled-down Berea sandstone

Shape	Triangle (%)	Square (%)	Circular (%)
Pore	0.909	0.089	0.002
Throat	0.835	0.148	0.017

In the simulation, we first simulate the primary drainage process until the capillary pressure reaches to 50MPa, and then reduce the capillary pressure stepwise until either of following conditions is satisfied (1) capillary pressure goes down to the preset minimum capillary pressure (here we set the minimum capillary pressure equal to -50MPa to enable a full imbibition cycle (spontaneous and forced imbibition); (2) water saturation equals 1.0; (3) no connected oil phase exists. The relative permeability and capillary pressure during the imbibition process are predicted in Fig. 20 and Fig. 21, respectively. As shown in Fig. 20, the capillary entry pressure during drainage becomes larger when the thin water film is included. Compared to NF (no thin water film exists) case, in DFC (dynamic thin water film with conductance) case, capillary pressure starts to rise dramatically at higher water saturation which illustrates due to the existence of thin water film non-wetting phase invades the smaller pores earlier. And due to the space occupied by thin water film, irreducible water saturation in DFC case is higher than that in NF case. In imbibition process, water invasion ends when there no longer exists available oil to displace and at that time capillary pressure is still positive which suggests that forced imbibition doesn't occur. DFC case has a lower residue oil saturation than NF case. That's because the trapped pore throat elements which contain oil are almost the same for two cases, while thin water films occupy considerable amount of space in these elements and result in lower residue oil saturation. We also found neglecting thin water film in tight porous media will overestimate the displacement efficiency (53.8% for NF case and 46.5% for DFC case). This can be explained by the increased probability of snap off by thin water film swelling.

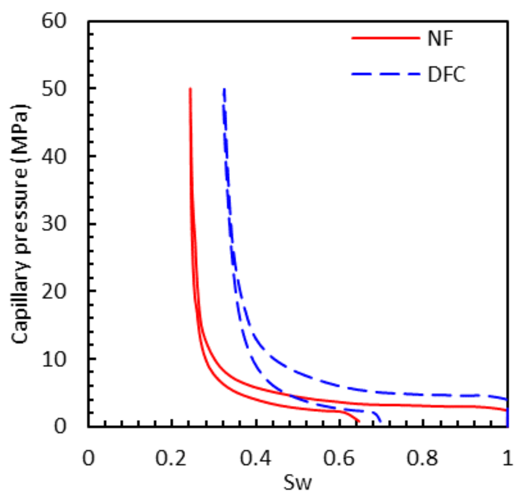

Fig. 20 Nanoscale effects on capillary pressure during imbibition. NF: no thin water film; DFC: dynamic thin water film with conductance

As shown in Fig. 21, for a given water saturation, the existence of thin water films attached to the water-wet rock surface reduces the water relative permeability and improves the oil phase relative permeability; this is due to the significant amount of water contributes to water saturation existing in thin water films, while thin films have very limited conductivity and oil phase occupying more central part has higher conductivity as seen in Fig. 22. The existence of nano-scale thin water film also increases the connate water saturation and reduces the oil phase permeability at connate water saturation during primary drainage process; for example, the connate water saturation increases from 0.22 to 0.42, and the associated oil relative permeability reduces from 0.99 to 0.90 when the thin water film is considered. On the contrast, it reduces the residual oil saturation and improves the associated water relative permeability significantly. As shown in Fig. 21a, the residue oil saturation changes from 0.36 to 0.31 and the water relative permeability at residue oil saturation changes from 0.17 to 0.21 if the thin water film is considered. Fig. 21b presents the normalized relative permeability predicted by two models. It is found that thin water film has almost no effect on normalized relative permeability. This is because thin water film mainly changes the conductivity and phase saturation and has limited effect on displacement sequence.

Except for its contribution to saturation and conductivity, thin water film could also increase connectivity of water phase especially in porous media consisting of circular shaped pores and throats. Previous pore network models [38, 88, 99] assumed circular shaped pores only contain one single fluid, however due to a considerable amount of thin water film in tight formation its contribution to connectivity should be included in circular shaped pores. Because reconstructed Berea sandstone only has few circular shaped pores, we employ the stochastic method to generate the pore network which only contains circular shaped pores and throats. As shown in Fig. 23, thin water films enhance the water phase connectivity and thus resulting in higher water relative permeability. At the same time, non-wetting phase displaces more wetting phase and obtain higher relative permeability at connate water saturation.

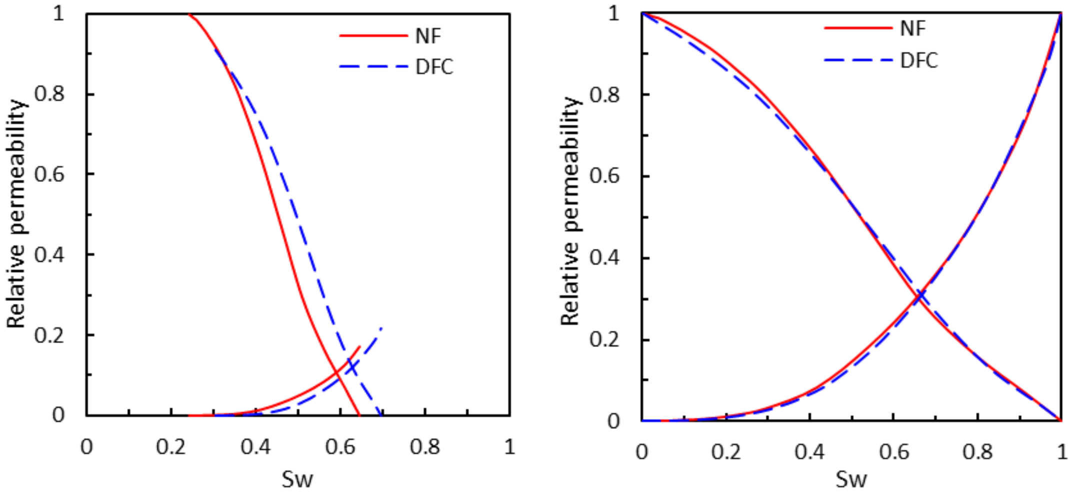

（a） Relative permeability curves (b) Normalized relative permeability curves

Fig. 21 The influence of thin water film on relative permeability during imbibition

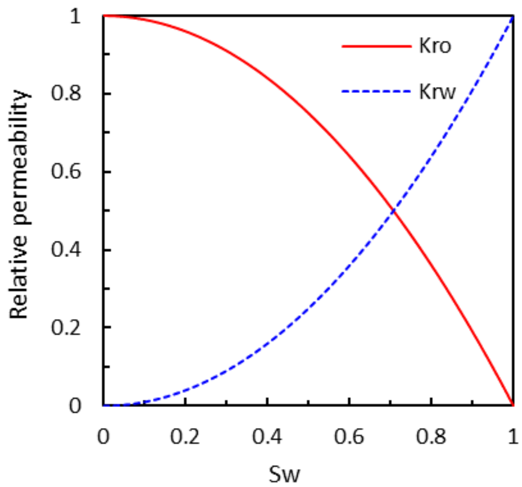

Fig. 22 Relative permeability curves in a tube

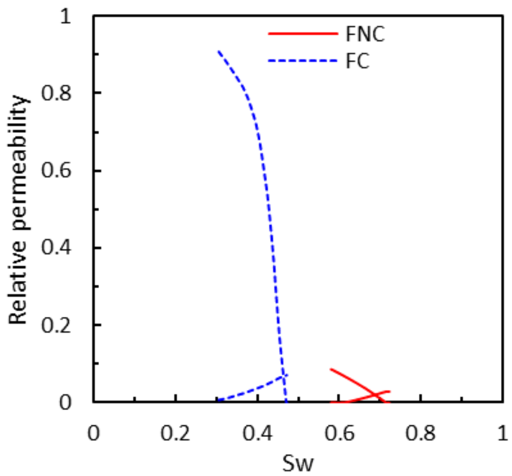

Fig. 23 Relative permeability curves during imbibition in porous media of circular shaped pores

(FC – considering water film connectivity; FNC – without considering water film connectivity)

Previous relative permeability models also consider water film thickness as a constant thickness [22, 31], thus here we also simulated the relative permeability using pore network modeling cooperated with a thin water film whose thickness remains constant. As shown in Fig. 24, the connate water saturation in the dynamic water film (DFC) case is lower than static water film (FC) case due to the thinning of water film that has been considered in the dynamic thin film model. In imbibition process, since the critical thickness of water film is larger than initial state, the residue oil saturation in DFC case has a lower value than that in FC case.

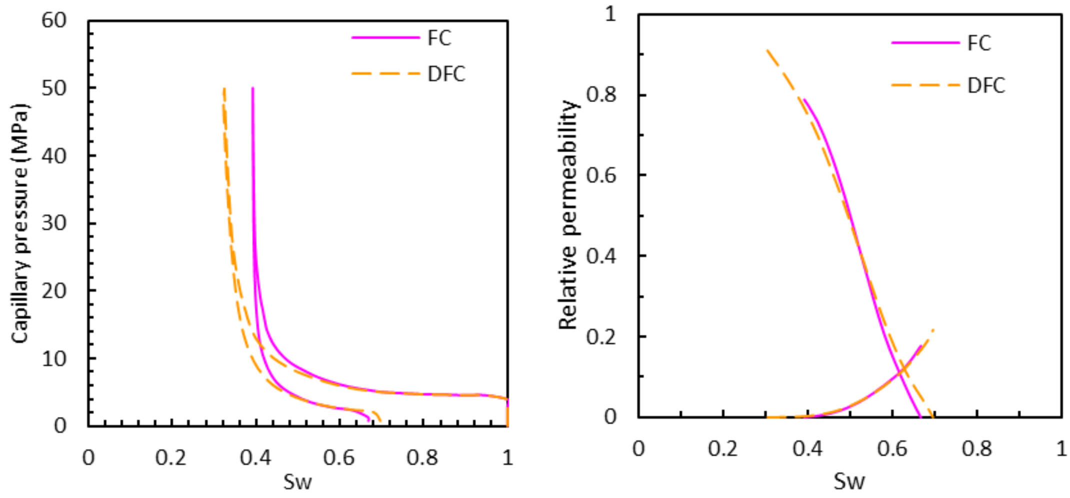

(a) Capillary pressure curves (b) Relative permeability curves

Fig. 24 Effect of water film thickness variation on capillary pressure curves and relative permeability curves (FC – constant water film thickness, DFC – dynamic water film thickness)

3.6. Discussion

Our present work has characterized the effect of thin water film on the relative permeability in tight porous media, and it has also clarified at which scale the thin water film should be considered.

However, it has to be noticed that out that our model is limited in water-wet porous media where the thin water film exists. When the wettability changes (such as oil-wet or mix-wet porous media) or thin water film ruptures due to the adsorption of polar compounds, the deposition of organic matter and roughness of solid surface and so on [17, 20], the oil will contact with solid surface directly and our model becomes invalid. Zhou et al. [100] found that the water flooding performance depended strongly on initial water saturation at mixed-wet conditions. Besides, since we mainly focus on the effect of thin water film on relative permeability, a rather simple pore filling mechanism [85] is employed in our model which controls the displacing sequence in imbibition process and pore throat cross-sections are assumed to be regular. Ruspini et al. [57] proposed a more realistic pore filling method which proves to have better agreement with experimental fluid distribution. Zhou et al [101, 102] investigated the capillary entry pressure for pores whose cross-section is obtained directly from 2D SEM rock image. Furthermore, the effect of viscosity on multiphase flow behavior is not incorporated in our model due to the lack of viscous coupling which need to be investigated further [103].

Therefore, more simulation models are still required to reveal the two-phase flow characteristics in tight formations under mix-wet or oil-wet condition. And more accurate imbibition mechanism at nano-scale needs to be introduced into pore network model.

4. Conclusions

In this paper, a quasi-static pore network model considering the effect of the thin water film is developed to describe multiphase flow in tight formations. Berea sandstone experiments and corresponding network generated from reconstructed Berea sandstone are used to validate the accuracy and reliability of the model. Based on the developed pore network model, pore-scale flow characteristics in nano porous media and its effect on relative permeability are then studied. Furthermore, the critical size of the average pore radius when the water film has a significant influence on relative permeability is investigated. The main conclusions can be drawn as follows:

(1) The thin water film plays an important role in fluid flow behavior in nanoscale pores. With a decrease in pore radius, the thickness of thin water film attached to solid wall becomes thinner however its effect on water saturation becomes more significant. The contribution of thin water films to water saturation can be up to approximately 20% for angular pores and 30% for circular pores with radius of 20 nm. Besides when the size of pore radius is below 20 nm, considering no thin wetting film will underestimate the capillary entry

pressure. The relative water conductance increases with a decrease in pore size while oil phase conductance decreases.

(2) Water film plays an important role in the prediction of relative permeability when the average pore radius is smaller than 100 nm. When average pore size reduces, the connate water saturation increases while residual oil saturation and oil relative permeability at connate water saturation decrease. As porous media has more irregular pores, water relative permeability increases.

(3) Thin water film influences relative permeability in nano porous media through the variation in water saturation, the phase connectivity and the thin water film swelling and thinning. In a tight formation dominated by angular pores, the effect of thin water film on the connectivity is negligible as shown in our study. On the contrary, in a tight formation dominated by the circular shaped pores, the thin water film increases the connectivity of the water phase and results in higher oil relative permeability at the connate water saturation.

Nomenclature

$\prod(h)$ —— the disjoining pressure between surfaces, Pa;

$\prod_m(h)$ —— the van der Waals force per unit area between surfaces, Pa;

$\prod_{el}(h)$ —— the electrostatic forces between charged surfaces per unit area, Pa;

$\prod_{st}(h)$ —— the structural force between charged surfaces per unit area, Pa;

h —— the water film thickness, m;

A_{ows} —— the Hamaker constant in an oil-water-solid system, J;

A_{oo} —— the Hamaker constants of oil/oil via vacuum, Pa;

A_{ww} —— the Hamaker constants of water/water via vacuum, Pa;

A_{ss} —— the Hamaker constants of solid/solid via vacuum, Pa;

h —— the water film thickness, m;

l —— the London wavelength, m;

n_b —— the ion density in bulk phase, M;

k_B —— the Boltzman constant, J/K;

T —— the temperature, K;

ζ_1 —— the zeta potential at solid/water surface, V;

ζ_2 —— the zeta potential at water/oil interface, V;

A_k —— the coefficient for the structural force, Pa;

λ —— the decay length, m;

κ —— the Deby-Huckel reciprocal length, m^{-1};

e —— the electron charge, C;

ε_0 —— the dielectric permittivity of vacuum, F/m;

ε —— the relative permittivity of water, Dimensionless;

z —— the ion valence, Dimensionless;

P_o —— the oil phase pressure, Pa;

P_w —— the water phase pressure, Pa;

$S_{w,t}$ —— the water saturation of the network, Dimensionless;

$S_{w,i}$ —— the water saturation of a pore throat, Dimensionless;

V_i —— the volume of a pore throat, m^3;

N —— the total number of pores and throats, Dimensionless;

V_t —— the total volume of the network, m^3;

q_{ij} —— the flow rate between pore i and pore j, m^3/s;

g_{ij} —— the flow conductance between pore i and pore j, $m^2/(Pa \cdot s)$;

P_i —— the pressure of pore i, Pa;

P_j —— the pressure of pore i, Pa;

L_t —— the length of the throat connecting pore i and pore j, m;

L_i, L_j —— the lengths from the pore-throat interface to the pore center, m;

σ —— the oil/water interfacial tension, N/m;

R —— the radius of the tube, m;

r_{ow} —— the capillary radius of arc meniscus, m;

θ_{ow} —— the water-oil contact angle, degree;

G —— the shape factor of pore throat cross-section, Dimensionless;

A —— the area of pore throat cross-section, m^2;

L —— the perimeter of pore throat cross-section, m;

r_a —— the oil maximum inscribed radius, m;

n —— the corner number of the pore throat, Dimensionless;

α_k —— the corner half angle, degree;

A_o —— the area occupied by oil in a pore throat, m^2;

L_{ow} —— the length of the oil-water interface, m;

L_{os} —— the length of the solid-water interface, m;

L_{of} —— the length of the thin water film, m;

$\theta_{h,k}$ —— the hinging contact in a corner, degree;

θ_a —— the advancing contact angle, degree;

m —— the number of adjacent non-wetting phase filled throats, Dimensionless;

x_i —— the random weight coefficient number ranging from zero to one, Dimensionless;

K —— the permeability, m^2;

μ_p —— the fluid viscosity, Pa·s;

μ_w —— the viscosity of water phase, Pa·s;

μ_o —— the viscosity of oil phase, Pa·s;

G_c^* ——the shape factor with zero curvature on the oil-water interface, Dimensionless;

A_c —— the corner water area, m^2;

A_f —— the film water area, m^2;

Acknowledgment

We acknowledge the Beijing Natural Science Foundation of China (No. 2204093), Science Foundation of China University of Petroleum, Beijing (No.2462018YJRC033) and financial support from China Scholarship Council ((No. 201906440134). Dr. Yingfang Zhou would like to acknowledge the support from State Key Laboratory of Oil and Gas Reservoir Geology and Exploitation (Southwest Petroleum University), PLN201602.

Appendix: Calculation of capillary entry pressure in angular pores

In order to account for the thin water film, we have modified the inscribe maximum circle r_a=R-h to calculate the capillary entry pressure.

Oil invasion scenario for polygon-shaped duct is sketched in Fig. A 1. Taken remaining thin water film into consideration, the oil phase doesn't contact solid surface directly.

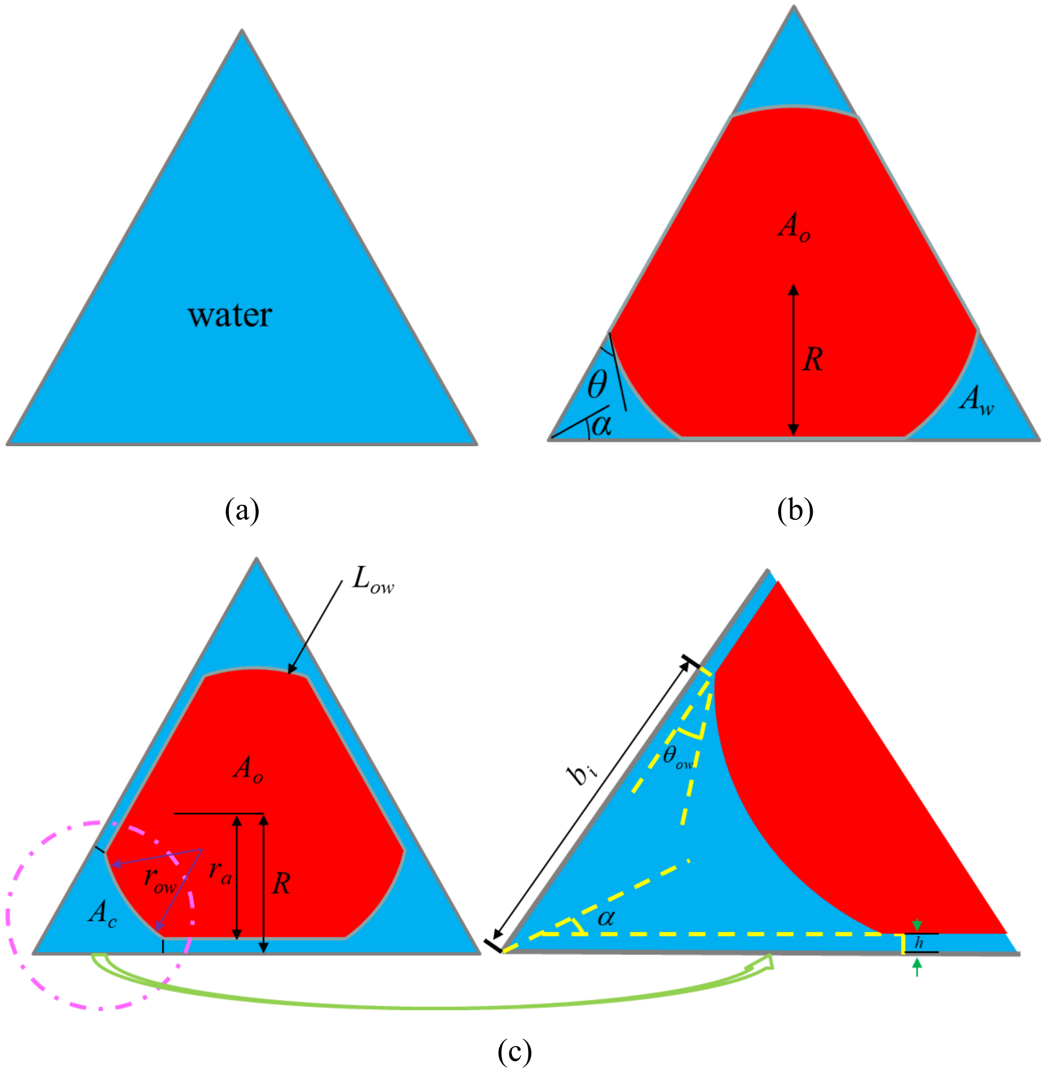

Fig. A 1 Three fluid configurations (a) initial state (b) drainage process without water films (c) drainage process with water films. Blue-water phase, red-oil phase.

Based on MS-P method [104], the entry capillary pressure for polygon shaped elements can be found from:

$$-\frac{\Delta A_o}{r_{ow}} + \cos\theta_{ow}\,\Delta L_{os} + \Delta L_{ow} = 0 \tag{A1}$$

where A_o is the oil phase area, θ_{ow} is the contact angle, r_{ow} is the capillary radius of arc meniscus, L_{os} is the length of oil-solid interface and L_{ow} is the length of oil-water interface. For convenience we define r_a=R-h, the interface lengths and oil phase area can be calculated from elementary geometry as follows:

$$A_o = \frac{r_a^2}{4G} - \sum_{k=1}^{n} r_{ow}^2 \left\{\theta_{ow} + \alpha_k - \frac{\pi}{2} + \cos(\theta_{ow})\frac{\cos(\theta_{ow}+\alpha_k)}{\cos(\alpha_k)}\right\} = \frac{r_a^2}{4G} - r_{ow}^2 S_1 \tag{A2}$$

$$L_{ow} = 2r_{ow}\sum_{k=1}^{n}\left\{\frac{\pi}{2} - \theta_{ow} - \alpha_k\right\} + \frac{r_a}{2G} - 2r_{ow}\sum_{k=1}^{n}\frac{\cos(\theta_{ow}+\alpha_k)}{\sin(\alpha_k)} = r_{ow}S_3 + \frac{r_a}{2G} - 2r_{ow}S_2 \tag{A3}$$

$$L_{os} = 0 \tag{A4}$$

where n is the total number of corners containing arc meniscus, α_k is half corner angle at corner k and G is the shape factor. The entry capillary pressure is then given by Eq. (A5).

$$P_c = \frac{\sigma(\sqrt{1+4GD}+1)}{r_a} \tag{A5}$$

where

$$D = \sum_{k=1}^{n}\left\{\frac{\pi}{2} - \theta_{ow} - \alpha_k\right\} + cos\,\theta_{ow}\sum_{k=1}^{n}\frac{cos(\theta_{ow}+\alpha_k)}{sin(\alpha_k)} \tag{A6}$$

References

[1] Zhou X, Wang Y, Zhang L, et al. Evaluation of enhanced oil recovery potential using gas/water flooding in a tight oil reservoir. Fuel 2020;272:117706.

[2] Luo Q, Gong L, Qu Y, et al. The tight oil potential of the Lucaogou Formation from the southern Junggar Basin, China. Fuel 2018;234:858-71.

[3] Cheng Z, Wang Q, Ning Z, et al. Experimental Investigation of Countercurrent Spontaneous Imbibition in Tight Sandstone Using Nuclear Magnetic Resonance. Energy & Fuels 2018;32(6):6507-17.

[4] Zhao H, Ning Z, Zhao T, et al. Effects of mineralogy on petrophysical properties and permeability estimation of the Upper Triassic Yanchang tight oil sandstones in Ordos Basin, Northern China. Fuel 2016;186:328-38.

[5] Gao H, Cao J, Wang C, et al. Comprehensive characterization of pore and throat system for tight sandstone reservoirs and associated permeability determination method using SEM, rate-controlled mercury and high pressure mercury. Journal of Petroleum Science and Engineering 2019;174:514-24.

[6] Gong Y, Liu K. Pore throat size distribution and oiliness of tight sands-A case study of the Southern Songliao Basin, China. Journal of Petroleum Science and Engineering 2020;184:106508.

[7] Zhao H, Zhao T, Ning Z, et al. Petrophysical characterization of tight oil sandstones by microscale X-ray computed tomography. Marine and Petroleum Geology 2019;102:604-14.

[8] Liu X, Wang J, Ge L, et al. Pore-scale characterization of tight sandstone in Yanchang Formation Ordos Basin China using micro-CT and SEM imaging from nm- to cm-scale. Fuel 2017;209:254-64.

[9] Chen M, Dai J, Liu X, et al. Effect of displacement rates on fluid distributions and dynamics during water flooding in tight oil sandstone cores from nuclear magnetic resonance (NMR). Journal of Petroleum Science and Engineering 2020;184:106588.

[10] Roman S, Abu-Al-Saud MO, Tokunaga T, et al. Measurements and simulation of liquid films during drainage displacements and snap-off in constricted capillary tubes. Journal of Colloid and Interface Science 2017;507:279-89.

[11] Li Z, He S. Influence of boundary layers upon filtration law in low-permeability oil reservoirs. Petroleum Geology & Oilfield Development in Daqing 2005;2.

[12] Tian X, Cheng L, Yan Y, et al. An improved solution to estimate relative permeability in tight oil reservoirs. Journal of Petroleum Exploration and Production Technology 2014;5(3):305-14.

[13] Xie Q, Saeedi A, Pooryousefy E, et al. Extended DLVO-based estimates of surface force in low salinity water flooding. Journal of Molecular Liquids 2016;221:658-65.

[14] Busireddy C, Rao DN. Application of DLVO Theory to Characterize Spreading in Crude oil-Brine-Rock Systems. *SPE/DOE Symposium on Improved Oil Recovery.* Tulsa, Oklahoma: Society of Petroleum Engineers; 2004:12.

[15] Takagishi H, Masuda T, Shimoda T, et al. Method for the Calculation of the Hamaker Constants of Organic Materials by the Lifshitz Macroscopic Approach with Density Functional Theory. The Journal of Physical Chemistry A 2019;123(40):8726-33.

[16] Hirasaki GJ. Wettability: Fundamentals and Surface Forces. SPE-17367-PA 1991;6(02):217-26.

[17] Rücker M, Bartels WB, Garfi G, et al. Relationship between wetting and capillary pressure in a crude oil/brine/rock system: From nano-scale to core-scale. Journal of Colloid and Interface Science 2020;562:159-69.

[18] Mahani H, Menezes R, Berg S, et al. Insights into the Impact of Temperature on the Wettability Alteration by Low Salinity in Carbonate Rocks. Energy & Fuels

2017;31(8):7839-53.

[19] Kumar D, Biswas SK. Contribution of different physical forces to the disjoining pressure of a thin water film being pressed by an oil droplet. Journal of Colloid and Interface Science 2010;348(1):255-64.

[20] Anderson WG. Wettability Literature Survey- Part 1: Rock/Oil/Brine Interactions and the Effects of Core Handling on Wettability. Journal of Petroleum Technology 1986;38(10):1125-44.

[21] Zhan S, Su Y, Jin Z, et al. Effect of water film on oil flow in quartz nanopores from molecular perspectives. Fuel 2020;262:116560.

[22] Zhang T, Li X, Sun Z, et al. An analytical model for relative permeability in water-wet nanoporous media. Chemical Engineering Science 2017;174(Supplement C):1-12.

[23] Chen M, Cheng L, Wang X, et al. Pore network modelling of fluid flow in tight formations considering boundary layer effect and media deformation. Journal of Petroleum Science and Engineering 2019;180:643-59.

[24] Cao RY, Wang Y, Cheng LS, et al. A New Model for Determining the Effective Permeability of Tight Formation. Transport in Porous Media 2016;112(1):21-37.

[25] Feng D, Li X, Wang X, et al. Water adsorption and its impact on the pore structure characteristics of shale clay. Applied Clay Science 2018;155:126-38.

[26] Bentsen RG, Manai AA. On the use of conventional cocurrent and countercurrent effective permeabilities to estimate the four generalized permeability coefficients which arise in coupled, two-phase flow. Transport in Porous Media 1993;11(3):243-62.

[27] Xu J, Guo C, Jiang R, et al. Study on relative permeability characteristics affected by displacement pressure gradient: Experimental study and numerical simulation. Fuel 2016;163:314-23.

[28] Li Y, Li H, Chen S, et al. Capillarity characters measurement and effects analysis in different permeability formations during waterflooding. Fuel 2017;194:129-43.

[29] Durucan S, Ahsan M, Shi J-Q, et al. Two phase relative permeabilities for gas and water in selected European coals. Fuel 2014;134:226-36.

[30] Finsterle S. Using the continuum approach to model unsaturated flow in fractured rock. Water Resources Research 2000;36(8):2055-66.

[31] Wang H, Su Y, Wang W, et al. Relative permeability model of oil-water flow in nanoporous media considering multi-mechanisms. Journal of Petroleum Science and Engineering 2019;183.

[32] Wang J, Song H, Rasouli V, et al. An integrated approach for gas-water relative permeability determination in nanoscale porous media. Journal of Petroleum Science and Engineering 2019;173:237-45.

[33] Li T, Song H, Wang J, et al. An analytical method for modeling and analysis gas-water relative permeability in nanoscale pores with interfacial effects. International Journal of Coal Geology 2016;159:71-81.

[34] Zhao H, Hu J, Wang J, et al. A comprehensive model for calculating relative permeability based on spontaneous imbibition and CT scanning measurement. Fuel 2019;247:287-93.

[35] Wang J, Song H, Wang Y. Investigation on the micro-flow mechanism of enhanced oil recovery by low-salinity water flooding in carbonate reservoir. Fuel 2020;266:117156.

[36] Fatt I. The Network Model of Porous Media. Society of Petroleum Engineers; 1956:38.

[37] Piri M, Blunt MJ. Three-dimensional mixed-wet random pore-scale network modeling of two- and three-phase flow in porous media. I. Model description. Physical Review E 2005;71(2):026301.

[38] Raeini AQ, Bijeljic B, Blunt MJ. Generalized network modeling of capillary-dominated two-phase flow. Physical Review E 2018;97(2):023308.

[39] Martínez-Mendoza EG, Díaz-Viera MA, Coronado M, et al. Capillary pressure and relative permeability estimation for low salinity waterflooding processes using pore network models. Journal of Petroleum Science and Engineering 2019;182.

[40] Yassin MR, Dehghanpour H, Wood J, et al. A Theory for Relative Permeability of Unconventional Rocks With Dual-Wettability Pore Network. SPE Journal 2016;21(06):1970-80.

[41] Burdine NT. Relative Permeability Calculations From Pore Size Distribution Data. Journal of Petroleum Technology 1953;5(03):71-8.

[42] Dong MZ, Dullien FAL, Dai LM, et al. Immiscible displacement in the interacting capillary bundle model - Part I. Development of interacting capillary bundle model. Transport in Porous Media 2005;59(1):1-18.

[43] Ahrenholz B, Tölke J, Krafczyk M. Lattice-Boltzmann simulations in reconstructed parametrized porous media. International Journal of Computational Fluid Dynamics 2006;20(6):369-77.

[44] Gunde A, Babadagli T, Roy SS, et al. Pore-scale interfacial dynamics and oil–water relative permeabilities of capillary driven counter-current flow in fractured porous media. Journal of Petroleum Science and Engineering 2013;103:106-14.

[45] Blunt MJ. Multiphase Flow in Permeable Media: A Pore-Scale Perspective. Cambridge: Cambridge University Press; 2017.

[46] Chen X, Zhou Y. Applications of digital core analysis and hydraulic flow units in petrophysical characterization. Advances in Geo-Energy Research 2017;1(1):18-30.

[47] Al-Kharusi AS, Blunt MJ. Multiphase flow predictions from carbonate pore space images using extracted network models. Water Resources Research 2008;44(6).

[48] Saif T, Lin Q, Butcher AR, et al. Multi-scale multi-dimensional microstructure imaging of oil shale pyrolysis using X-ray micro-tomography, automated ultra-high resolution SEM, MAPS Mineralogy and FIB-SEM. Applied Energy 2017;202:628-47.

[49] Blunt MJ, Bijeljic B, Dong H, et al. Pore-scale imaging and modelling. Advances in Water Resources 2013;51:197-216.

[50] Blunt MJ, Jackson MD, Piri M, et al. Detailed physics, predictive capabilities and macroscopic consequences for pore-network models of multiphase flow. Advances in Water Resources 2002;25(8-12):1069-89.

[51] Golparvar A, Zhou Y, Wu K, et al. A comprehensive review of pore scale modeling methodologies for multiphase flow in porous media. Advances in Geo-Energy Research 2018;2(4):418-40.

[52] Roslin A, Pokrajac D, Wu K, et al. 3D pore system reconstruction using nano-scale

2D SEM images and pore size distribution analysis for intermediate rank coal matrix. Fuel 2020;275:117934.

[53] Dullien FA. Porous media: fluid transport and pore structure. Academic press; 2012.

[54] Nguyen VH, Sheppard AP, Knackstedt MA, et al. The effect of displacement rate on imbibition relative permeability and residual saturation. Journal of Petroleum Science and Engineering 2006;52(1):54-70.

[55] van Dijke MIJ, Sorbie KS. Pore-scale network model for three-phase flow in mixed-wet porous media. Physical Review E 2002;66(4):046302.

[56] Oren PE, Bakke S, Arntzen OJ. Extending Predictive Capabilities to Network Models. SPE Journal 1998;3(04):324-36.

[57] Ruspini LC, Farokhpoor R, Øren PE. Pore-scale modeling of capillary trapping in water-wet porous media: A new cooperative pore-body filling model. Advances in Water Resources 2017;108:1-14.

[58] Wang XK, Sheng JJ. Pore network modeling of the Non-Darcy flows in shale and tight formations. Journal of Petroleum Science and Engineering 2018;163:511-8.

[59] Wang XK, Sheng JJ. Spontaneous imbibition analysis in shale reservoirs based on pore network modeling. Journal of Petroleum Science and Engineering 2018;169:663-72.

[60] Cui R, Feng Q, Chen H, et al. Multiscale random pore network modeling of oil-water two-phase slip flow in shale matrix. Journal of Petroleum Science and Engineering 2019;175:46-59.

[61] Yang L, Qun L, Xiangui L, et al. Characteristics of micro scale nonlinear filtration. Petroleum Exploration and Development 2011;38(3):336-40.

[62] Tokunaga TK, Wan J. Water film flow along fracture surfaces of porous rock. Water Resources Research 1997;33(6):1287-95.

[63] Feng D, Wu K, Wang X, et al. Modeling the confined fluid flow in micro-nanoporous media under geological temperature and pressure. Int J Heat Mass Transf 2019;145:118758.

[64] Kaminsky R, Radke CJ. Asphaltenes, Water Films, and Wettability Reversal. SPE

Journal 1997;2(04):485-93.

[65] Hammond PS. Nonlinear adjustment of a thin annular film of viscous fluid surrounding a thread of another within a circular cylindrical pipe. Journal of Fluid Mechanics 1983;137:363-84.

[66] Roof JG. Snap-Off of Oil Droplets in Water-Wet Pores. Society of Petroleum Engineers Journal 1970;10(01):85-90.

[67] Huerre A, Theodoly O, Leshansky AM, et al. Droplets in Microchannels: Dynamical Properties of the Lubrication Film. Physical Review Letters 2015;115(6):064501.

[68] Derjaguin BV, Churaev NV, Muller VM. The Derjaguin—Landau—Verwey—Overbeek (DLVO) Theory of Stability of Lyophobic Colloids. In: Derjaguin BV, Churaev NV, Muller VM, editors. Surface Forces. Boston, MA: Springer US; 1987, p. 293-310.

[69] Brooks DE, Levine YK, Requena J, et al. Van der Waals forces in oil-water systems from the study of thin lipid films - III. Comparison of experimental results with Hamaker coefficients calculated from Lifshitz theory. Proceedings of the Royal Society of London A Mathematical and Physical Sciences 1975;347(1649):179-94.

[70] Israelachvili JN. Intermolecular and surface forces. Academic press; 2015.

[71] Melrose JC. Interpretation Of Mixed Wettability States In Reservoir Rocks. *SPE Annual Technical Conference and Exhibition.* New Orleans, Louisiana: Society of Petroleum Engineers; 1982:19.

[72] Gu Y. Experimental determination of the Hamaker constants for solid–water–oil systems. Journal of Adhesion Science and Technology 2001;15(11):1263-83.

[73] Li J, Chen Z, Wu K, et al. Effect of water saturation on gas slippage in circular and angular pores. AIChE Journal 2018;64(9):3529-41.

[74] Zhou Y, Helland JO, Hatzignatiou DG. Computation of three-phase capillary entry pressures and arc menisci configurations in pore geometries from 2D rock images: A combinatorial approach. Advances in Water Resources 2014;69:49-64.

[75] Mayer RP, Stowe RA. Mercury porosimetry—breakthrough pressure for penetration between packed spheres. Journal of Colloid Science 1965;20(8):893-

911.

[76] Princen HM. Capillary phenomena in assemblies of parallel cylinders: I. Capillary rise between two cylinders. Journal of Colloid and Interface Science 1969;30(1):69-75.

[77] Princen HM. Capillary phenomena in assemblies of parallel cylinders: II. Capillary rise in systems with more than two cylinders. Journal of Colloid and Interface Science 1969;30(3):359-71.

[78] Princen HM. Capillary phenomena in assemblies of parallel cylinders: III. Liquid Columns between Horizontal Parallel Cylinders. Journal of Colloid and Interface Science 1970;34(2):171-84.

[79] Princen HM. Capillary pressure behavior in pores with curved triangular cross-section: Effect of wettability and pore size distribution. Colloids and Surfaces 1992;65(2):221-30.

[80] Ma S, Mason G, Morrow NR. Effect of contact angle on drainage and imbibition in regular polygonal tubes. Colloids and Surfaces A: Physicochemical and Engineering Aspects 1996;117(3):273-91.

[81] Lago M, Araujo M. Threshold Pressure in Capillaries with Polygonal Cross Section. Journal of Colloid and Interface Science 2001;243(1):219-26.

[82] Zhou Y. Pore scale modeling of capillary pressure curves in 2D rock images. University of Stavanger, Norway; 2013.

[83] Jerauld GR, Salter SJ. The effect of pore-structure on hysteresis in relative permeability and capillary pressure: Pore-level modeling. Transport in Porous Media 1990;5(2):103-51.

[84] Blunt MJ. Pore Level Modeling of the Effects of Wettability. SPE Journal 1997;2(04):494-510.

[85] Blunt MJ. Physically-based network modeling of multiphase flow in intermediate-wet porous media. Journal of Petroleum Science and Engineering 1998;20(3-4):117-25.

[86] Ryazanov AV, van Dijke MIJ, Sorbie KS. Two-Phase Pore-Network Modelling: Existence of Oil Layers During Water Invasion. Transport in Porous Media

2009;80(1):79-99.

[87] Reza J, Martin H. Analytical and numerical studies of separated laminar two-phase flow in elliptical ducts of arbitrary axis ratio: Analytische und numerische Studien separierter laminarer Zweiphasenströmungen in Kanälen elliptischen Querschnitts mit beliebigem Achsenverh/:altnis. Chemical Engineering and Processing: Process Intensification 1988;24(3):121-32.

[88] Valvatne PH. Predictive pore-scale modelling of multiphase flow. Department of Earth Science and Engineering, Imperial College London; 2004.

[89] Spurk JH, Aksel N. Fluid mechanics. Berlin: Springer; 2008.

[90] Lerdahl TR, Oren P-E, Bakke S. A predictive network model for three-phase flow in porous media. *SPE/DOE Improved Oil Recovery Symposium.* Society of Petroleum Engineers; 2000.

[91] Dong H, Blunt MJ. Pore-network extraction from micro-computerized-tomography images. Physical Review E 2009;80(3):036307.

[92] Morrow NR. The Effects of Surface Roughness On Contact: Angle With Special Reference to Petroleum Recovery. Journal of Canadian Petroleum Technology 1975;14(04):13.

[93] Gharbi O, Blunt MJ. The impact of wettability and connectivity on relative permeability in carbonates: A pore network modeling analysis. Water Resources Research 2012;48(12).

[94] Oak MJ. Three-Phase Relative Permeability of Water-Wet Berea. *SPE/DOE Enhanced Oil Recovery Symposium.* Tulsa, Oklahoma: Society of Petroleum Engineers; 1990:12.

[95] Mattia D, Starov V, Semenov S. Thickness, stability and contact angle of liquid films on and inside nanofibres, nanotubes and nanochannels. Journal of Colloid and Interface Science 2012;384(1):149-56.

[96] Li J, Li X, Wu K, et al. Thickness and stability of water film confined inside nanoslits and nanocapillaries of shale and clay. International Journal of Coal Geology 2017;179:253-68.

[97] Torskaya TS, Jin G, Torres-Verdin C. Pore-Level Analysis of the Relationship

Between Porosity, Irreducible Water Saturation, and Permeability of Clastic Rocks. *SPE Annual Technical Conference and Exhibition.* Anaheim, California, U.S.A.: Society of Petroleum Engineers; 2007:9.

[98] Singh K, Bultreys T, Raeini AQ, et al. Imbibition in porous media: correlations of displacement events with pore-throat geometry and the identification of a new type of pore snap-off. 2019.

[99] Al-Gharbi MS, Blunt MJ. Dynamic network modeling of two-phase drainage in porous media. Phys Rev E Stat Nonlin Soft Matter Phys 2005;71(1 Pt 2):016308.

[100] Zhou Y, Helland J, Hatzignatiou DG. Pore-Scale Modeling of Waterflooding in Mixed-Wet-Rock Images: Effects of Initial Saturation and Wettability. SPE Journal 2014;19(01):88-100.

[101] Zhou Y, Hatzignatiou DG, Helland JO. On the estimation of CO2 capillary entry pressure: Implications on geological CO2 storage. International Journal of Greenhouse Gas Control 2017;63:26-36.

[102] Yang J, Zhou Y. An Automatic In Situ Contact Angle Determination Based on Level Set Method. Water Resources Research 2020;56(7):e2020WR027107.

[103] Xie C, Raeini AQ, Wang Y, et al. An improved pore-network model including viscous coupling effects using direct simulation by the lattice Boltzmann method. Advances in Water Resources 2017;100:26-34.

[104] Shahrak AZ. Pore-scale network modeling of two-and three-phase flow based on thermodynamically consistent threshold capillary pressures. University of Wyoming; 2014.